The yeast Arf-GAP Glo3p is required for the endocytic recycling of cell surface proteins

Authors

Daiki Kawada[1], Hiromu Kobayashi[1], Tsuyoshi Tomita[1], Eisuke Nakata[1], Makoto Nagano[1,2], Daria Elisabeth Siekhaus[3], Junko Y. Toshima[2,4,5], and Jiro Toshima[1,2,5]

Affiliations

[1]Department of Biological Science and Technology, Tokyo University of Science, Niijuku 6-3-1, Katsushika-ku, Tokyo 125-8585, Japan

[2]Research Center for RNA Science, RIST, Tokyo University of Science, Niijuku 6-3-1, Katsushika-ku, Tokyo 125-8585, Japan

[3]Institute of Science and Technology Austria, Am Campus 1, A-3400 Klosterneuburg, Austria

[4]Faculty of Science and Engineering, Waseda University, Wakamatsu-cho 2-2, Shinjuku-ku, Tokyo 162-8480, Japan

[5]Corresponding authors:

Telephone 81-3-5876-1501, Fax 81-3-5876-1464, email jtosiscb@rs.noda.tus.ac.jp

Telephone 81-3-5369-7300, Fax 81-3-5876-1464, email yama_jun@aoni.waseda.jp

Abstract

Small GTP-binding proteins of the Ras superfamily play diverse roles in intracellular trafficking. Among them, the Rab, Arf, and Rho families function in successive steps of vesicle transport, in forming vesicles from donor membranes, directing vesicle trafficking towards target membranes and docking vesicles onto target membranes. These proteins act as molecular switches that are controlled by a cycle of GTP binding and hydrolysis regulated by guanine nucleotide exchange factors (GEFs) and GTPase-activating proteins (GAPs). In this study we explored the role of GAPs in the regulation of the endocytic pathway using fluorescently labeled yeast mating pheromone α-factor. Among 25 non-essential GAP mutants, we found that deletion of the *GLO3* gene, encoding Arf-GAP protein, caused defective internalization of fluorescently labeled α-factor. Quantitative analysis revealed that *glo3*Δ cells show defective α-factor binding to the cell surface. Interestingly, Ste2p, the α-factor receptor, was mis-localized from the plasma membrane to the vacuole in *glo3*Δ cells. Domain deletion mutants of Glo3p revealed that a GAP-independent function, as well as the GAP activity, of Glo3p is important for both α-factor binding and Ste2p localization at the cell surface. Additionally, we found that deletion of the *GLO3* gene affects the size and number of Arf1p-residing Golgi compartments and causes a defect in transport from the TGN to the plasma membrane. Furthermore, we demonstrated that *glo3*Δ cells were defective in the late endosome-to-TGN transport pathway, but not in the early endosome-to-TGN transport pathway. These findings suggest novel roles for Arf-GAP Glo3p in endocytic recycling of cell surface proteins.

Keywords

Arf-GAP, small GTPase, vesicular trafficking, intracellular trafficking, endocytosis

Abbreviations

GAP, GTPase-activating protein; GFP, green fluorescent protein; mCherry, monomeric Cherry; GEF, guanine nucleotide exchange factor; VPS, vacuolar protein sorting; TGN, *trans*-Golgi network; ER, endoplasmic reticulum

1. Introduction

Endocytosis of membrane proteins and lipids is a process critical for a wide variety of functions as well as the survival of eukaryotic cells. Upon internalization from the plasma membrane, cargo proteins such as cell surface receptors are usually delivered to the early endosome. Subsequently they can be sorted to recycling endosomes that bring the cargo back to the plasma membrane, or to late endosomes/multivesicular bodies en route to the lysosome/vacuole for degradation. Studies of yeast and mammalian cells have shown that these successive steps of vesicular trafficking are strictly regulated by various small GTPase proteins, including Rho, Rab, and Arf/Sar, and that the fundamental roles of these proteins in vesicular trafficking are conserved throughout eukaryotes [1]. These small GTPase proteins act as molecular switches that cycle between two conformational states: an inactive, GDP-bound state and an active, GTP-bound state. Guanine nucleotide exchange factors (GEFs) activate the switch by catalyzing the exchange of GDP for GTP, whereas GTPase-activating proteins (GAPs) increase the intrinsic GTPase activity and inactivate the switch [2].

Arf proteins undergo a cycle of GTP binding and hydrolysis to regulate vesicle formation on a variety of donor membranes, such as those of the Golgi, endosomes, and plasma membrane [3-5]. In mammals, Arf proteins can be divided into three classes based on their amino acid sequence similarity: class I (ARF1 and ARF3), class II (ARF4 and ARF5), and class III (ARF6) [6]. Class I and II Arfs localize primarily to the Golgi apparatus and function there and in compartments along the

secretory pathway. The Class III Arf6 functions mainly at the plasma membrane and has roles in endocytic trafficking [7].

Budding yeast has three *ARF* genes: *ARF1*, *ARF2*, and *ARF3*. Arf1p and Arf2p, are 96% identical and serve as functional homologues, although the level of protein produced from *ARF1* is ~10-fold higher than that from *ARF2* [8]. Through their roles in coat assembly and disassembly, Arf1p and Arf2p are known to facilitate COPI and clathrin coat dynamics on the Golgi apparatus and function in many different steps of intracellular trafficking, such as retrograde transport from the Golgi to the ER and anterograde transport to the lysosome/vacuole [7, 9, 10]. Previous studies demonstrated that deletion of the *ARF1* gene creates a defect in the secretory pathway, as evidenced by altered glycosylation of secreted proteins [11]. Additionally, recent studies have revealed a role for Arf1p in the exomer-mediated trafficking of cargo proteins from the *trans*-Golgi network (TGN) to the plasma membrane [12-15].

Yeast has six structurally related proteins with the potential to provide GAP activity for the Arf1 and Arf2 proteins [16-18]. Genetic studies have shown that the four known yeast Arf-GAPs have overlapping functions [19]. Two of these Arf-GAPs, Gcs1p and Glo3p, are essential for retrograde transport from the Golgi to the ER [17], however, Gcs1p makes only a small contribution, because *glo3*Δ cells exhibit severely defective retrograde transport, whereas *gcs1*Δ cells show only a minor defect [17]. Glo3p has been identified as a component of COPI vesicles, and a mutant version of Glo3p (Glo3-R59K) prevents the generation of COPI-coated transport vesicles *in vitro* [20]. It has also been reported that Gcs1p and Age2p mediate the formation and

function of TGN-derived transport vesicles destined for the vacuole via both the vacuolar protein sorting (VPS) and AP-3-dependent pathways [21]. However, the role of Arf-GAPs in regulating transport from the TGN to the plasma membrane in the secretory pathway has not been clarified.

In a previous study, we synthesized a fluorescently labeled mating pheromone derivative, which binds specifically to the Ste2p G protein-coupled receptor and is used as a marker for receptor-mediated endocytosis [22, 23]. In the present study, using this fluorescent marker, we show that cells lacking Glo3p exhibit defects in α-factor internalization. Quantitative analysis demonstrates that the *glo3*Δ mutant has a defect in α-factor binding to the cell surface. We also show that *glo3*Δ cells have defects in the late endosome-to-TGN transport pathway, and that therefore, endocytosed Ste2p is sorted to the vacuole, not to the plasma membrane via the recycling pathway. We extend these findings to Kex2p and Gap1p, demonstrating that Glo3 seems to play a general role in recycling cell surface and TGN resident proteins from the late endosome and thus preventing them from being turned over in the vacuole.

2. Material and Methods

2.1. Yeast strains, growth conditions, and plasmids

The yeast strains used in this study are listed in Table 1. Cells depleted of Arf-GAPs, Rab-GAPs, or Rho-GAPs were purchased from Open Biosystems and strain identities were confirmed by PCR using primers specific to the gene and the selection marker (Supplementary Fig. 1). All strains were grown in standard rich medium (YPD) or synthetic medium supplemented with 2% glucose (SD) and appropriate amino acids. The N-terminal GFP tag was integrated at the endogenous locus of the *GLO3* gene as follows: The GFP (S65T) fragment whose stop codon was replaced with a BglII site was subcloned into BamHI- and NotI-digested pBlueScript II SK (pBS-GFP), and the NotI-SacII fragment, which contains the *S. cerevisiae ADH1* terminator and the *His3MX6* module, was amplified by PCR using pFA6a-GFP (S65T)-HIS3MX6 as a template, and inserted into NotI- and SacII-digested pBS-GFP (pBS-GFP-HIS3). To create an integration plasmid, 300-bp 5' UTR of the *GLO3* gene and the N-terminal fragment of the *GLO3* ORF (nt 1-470) were generated by PCR and cloned into the BamHI or BglII site of pBS-GFP-HIS3. To integrate GFP at the N terminus of the *GLO3* gene, the integration plasmid was linearized by KpnI and transformed into yeast. C-terminal GFP or mCherry tagging of proteins was performed by PCR-based homologous recombination using pFA6a-GFP(S65T) or pFA6a-mCherry, respectively, as a template [24].

Glo3p and its domain deletion mutants were expressed from pRS316 plasmids in *glo3*Δ cells. The full-length *GLO3* gene was amplified by PCR from yeast genomic

DNA using primers 5’-CGGGATCCGCTGTTCCCCTGTTACTC-3’ and 5’-CGCTCGAGCAATTAGAAACAGAGATG-3’, and cloned into BamHI- and XhoI-digested pRS316. DNA fragments encoding GLO3ΔGAP (Glo3Δ2-145) or GLO3ΔBoCCS (Glo3Δ214-375) was created by PCR amplification from full-length *GLO3* gene using primers 5’-CACATAGCGACAATGAACGGTCAAGATTCTTCG GAC-3’ and 5’-AGAATCTTGACCGTTCATTGTCGCTATGTGTATAC-3’ or 5’-ACTGTCACTAAAACGGGCAGAATCGCGGAAAGGTAC-3’ and 5’-TTCCGCGATTCTGCCCGTTTTAGTGACAGTGGTCTTG-3’, respectively, and cloned into pRS316.

2.2. Fluorescence microscopy

Fluorescence microscopy was performed using an Olympus IX81 microscope equipped with a 100x/NA 1.40 (Olympus) objective and an Orca-AG cooled CCD camera (Hamamatsu), using Metamorph software (Universal Imaging). To assess colocalization with high precision, each image pair was acquired simultaneously using dual-channel 2D imaging system. Simultaneous imaging of red and green fluorescence was performed using an Olympus IX81 microscope, described above, and an image splitter (Dual-View; Optical Insights) that divided the red and green components of the images with a 565-nm dichroic mirror and passed the red component through a 630/50 nm filter and the green component through a 530/30 nm filter.

2.3. Fluorescence labeling of α-factor and endocytosis assays

Fluorescence labeling of α-factor was performed as described previously [22]. For endocytosis assays, cells were grown to an OD_{600} of ~0.5 in 0.5 ml YPD, briefly centrifuged, and resuspended in 20 μl SM with 5 μM Alexa Fluor 594-α-factor. After incubation on ice for 2 h, the cells were washed with ice-cold SM. Internalization was initiated by the addition of SM containing 4% glucose and amino acids at 25°C.

2.4. ^{35}S-labeled α-factor internalization assay

Preparation and internalization of ^{35}S-labeled α-factor was performed as described previously [25]. Briefly, cells were grown to an OD_{600} of ~0.3 in 50 ml YPD, briefly centrifuged and resuspended in 4 ml YPD containing 1% (w/v) BSA, 50 mM KH_2PO_4, pH 6, and 20 □g/ml of uracil, adenine, and histidine. After adding ^{35}S-labeled α-factor, cell aliquots were withdrawn at various time points and subjected to a wash in pH 1.1 buffer to remove surface-bound α-factor so that internalized α-factor could be measured, or in pH 6 buffer to determine the total amount (internalized and bound) of α-factor. The amount of cell-associated radioactivity after each wash was determined by scintillation counting. Each experiment was performed at least three times.

2.5. CPY colony blot assay

The CPY colony blot assay was performed as described previously [26]. After overnight growth in YPD medium, cells were diluted to 0.2 OD_{600}, and 2 μl of each dilution was spotted on a YPD plate. After incubation at 30°C for 2 days, a nitrocellulose filter was placed on the plate and then incubated at 30°C for 1 day. The

nitrocellulose filter was washed several times with standard phosphate-buffered saline. The membranes were then subjected to immunoblotting with mouse anti-CPY (Molecular Probes, Eugene, OR). The mouse anti-CPY was used at a 1:1000 dilution and donkey anti-mouse IgG-horseradish peroxidase (Amersham Biosciences, Piscataway, NJ) was used as the secondary antibody at a 1:2000 dilution, followed by visualization with enhanced chemiluminescence reagents (PerkinElmer Life Sciences, Boston, MA) in accordance with the manufacturer's protocols. Quantification of chemiluminescence signals was performed using a CCD camera (LAS 1000, FujiFilm) and the software programs Image Reader LAS 1000 V1.1 and Image Gauge V4.0 (FujiFilm).

3. Results

3.1. Identification of a GAP mutant with an endocytic pathway defect

Multiple GAPs have been implicated in the control of intracellular trafficking in both yeast and mammalian cells. Although 25 non-essential GAP genes have been identified in budding yeast, including Arf-GAP, Rab-GAP and Rho-GAP, the specific functions of these GAP proteins in the distinct pathways of intracellular trafficking have remained unclear. To identify the GAP(s) involved in the regulation of the endocytic pathway, we examined the transport of Alexa Fluor 594-labeled α-factor (A594-α-factor) to the vacuole. As reported previously, when added to cells, A594-α-factor was first localized to the plasma membrane and then mostly transported to the vacuole within 15 min (Fig. 1A, *left panel*) [22]. In contrast, cells depleted of End3p, which is required for the internalization step of endocytosis and actin cytoskeleton organization [27], exhibited defective internalization of A594-α-factor from the plasma membrane to the cytosol (Fig. 1A, *right panel*). When we examined the localization of A594-α-factor in cells depleted of Arf-GAPs, Rab-GAPs, or Rho-GAPs, we identified four mutants that exhibited differences in A594-α-factor localization from wild-type cells (Fig. 1B-D). Among them, three mutants – *gyp1*Δ, *gyp6*Δ, and *sac7*Δ – exhibited accumulation of A594-α-factor in aberrant fragmented vacuoles [28], but defective transport of A594-α-factor to the vacuole was not observed (Fig. 1C-E). In contrast, the *glo3*Δ mutant exhibited a severe defect in A594-α-factor internalization (Fig. 1B). Quantitative analysis of A594-α-factor localizaion also confirmed that the defective transport of A594-α-factor to the vacuole is specifically observed in the *glo3*Δ

mutant (Fig. 1E). These results suggest a specific role for Glo3p GAP in the early stages of the endocytic pathway.

3.2. Requirement for Glo3p for endocytic internalization

Among the Arf-GAPs, only Gts1p has been shown to localize to cortical patches and to be implicated in endocytic internalization, but *GTS1* single mutants show only minor defects in the endocytic pathway [29, 30]. Thus, our finding that *glo3*Δ cells show defective internalization of A594-α-factor prompted us to examine whether Glo3p and Gts1p have overlapping functions during endocytic internalization. To examine this possibility, we labeled wild-type, *glo3*Δ, and *gts1*Δ cells with A594-α-factor and followed the localization at several time points after α-factor internalization. While appreciable delays of α-factor internalization and transport were observed in *glo3*Δ and *glo3*Δ *gts1*Δ double-mutant cells, *gts1*Δ cells showed only a negligible defect in α-factor internalization although they showed slight delays of α-factor transport to the vacuole as described previously (Fig. 2A)[30]. To distinguish the localization of A594-α-factor at endosomes and at fragmented vacuoles, we also observed the transport of A594-α-factor in wild-type and *glo3*Δ cells expressing GFP-fused Pep4p, a vacuolar aspartyl protease. As shown in Supplementary Fig. 2A, the difference between A594-α-factor localization at endosomes and fragmented vacuoles was quite obvious in *glo3*Δ cells since the intensities of endosomes were much brighter than those of vacuoles. Quantitative analysis categorizing A594-α-factor localization as vacuole-only, endosome and vacuole, or plasma membrane revealed that *glo3*Δ and *glo3*Δ *gts1*Δ

double-mutant cells have obvious defects in α-factor transport, but that combining the *glo3*Δ and *gts1*Δ mutations has little additive effect, as the defect is not greater than that seen in the *glo3*Δ single mutants (Fig. 2B). We further examined the effect on endocytosis by assessing the internalization of ^{35}S-labeled α-factor. As shown in Fig. 2C, *glo3*Δ cells exhibited a defect in α-factor internalization, whereas *gts1*Δ cells had no apparent defect. Unexpectedly, this assay also revealed that membrane-bound and internalized ^{35}S-labeled α-factor at each time point was dramatically reduced in *glo3*Δ cells, compared to that in wild-type or *gts1*Δ cells (Fig. 2D and Supplementary Fig. 2B). These results suggest that the endocytic defects observed in *glo3*Δ cells could be due to decreased cell binding of α-factor.

3.3. Transport of the α-factor receptor, Ste2p, to the plasma membrane is impaired in *glo3*Δ cells

We next investigated whether decreased binding of α-factor to *glo3*Δ cells is related to the expression level of Ste2p, a receptor for α-factor, at the plasma membrane. Intriguingly, in *glo3*Δ cells, Ste2p localization was markedly shifted to intracellular compartments, in contrast to its association with the plasma membrane in wild-type cells (Fig. 3A). While ~95% of wild-type cells obviously exhibited Ste2-GFP at the plasma membrane as well as the vacuole, only around 33% of *glo3*Δ cells showed plasma membrane localization of Ste2p (Fig. 3B). Mutant cells expressing catalytically inactive Glo3 mutants (Glo3-R59K) [20] also exhibited some decrease in Ste2p localization at the plasma membrane (to ~67%) (Fig. 3B). Intracellular Ste2-GFP was

highly colocalized with mCherry-fused Pep4p in both wild-type and *glo3*Δ cells (Fig. 3C), indicating that inactivation of Glo3p leads to missorting of Ste2p from the plasma membrane to the vacuole. To clarify whether the decreased localization of Ste2p at the plasma membrane in *glo3*Δ cells is caused by a recycling defect, or simply by defective transport from the TGN to the plasma membrane, we examined the localization in *glo3*Δ cells of GFP-fused Ste2 lacking the C-terminal cytoplasmic region, which contains several endocytic signals essential for internalization (Ste2Δ300) [23]. In *glo3*Δ cells Ste2Δ300-GFP will be unable to be recycled in any case but should be delivered to the plasma membrane and not the vacuole as long as TGN to plasma membrane trafficking is normal. Localization of Ste2Δ300-GFP was observed at the plasma membrane and not the vacuole in both wild-type and *glo3*Δ cells although partial mis-localization of Ste2Δ300-GFP to the ER was also observed (Fig. 3D). As described previously [23], A594-α-factor was predominantly localized at the plasma membrane and showed little internalization into the cytosol (Fig. 3D). This result suggests that Ste2Δ300-GFP is transported to the plasma membrane but not internalized in *glo3*Δ cells (Fig. 3D). Thus in *glo3*Δ cells, TGN to plasma membrane transport appears normal and decreased localization of Ste2p at the plasma membrane seems to be caused by a recycling defect after endocytic internalization.

To further confirm that the reduction in α-factor binding was specific to *glo3*Δ cells, and absent in other Arf-GAP mutants, we compared ^{35}S-labeled α-factor binding among strains. As expected, binding of α-factor to *glo3*Δ cells was significantly decreased in comparison to other Arf-GAP mutants (Fig. 3E). *gcs1*Δ cells also exhibited

a slight but statistically insignificant decrease in the relative binding of ^{35}S-α-factor ($P > 0.05$) (Fig. 3E). We then examined the effect of a double mutant of *gcs1*Δ and *glo3-R59K* on binding of ^{35}S-α-factor and cell growth since these proteins were known to have overlapping functions [17]. As shown in Fig. 3E, we found that the binding of ^{35}S-α-factor to *glo3-R59K gcs1*Δ cells was also almost the same as that to the *glo3-R59K* cell. Additionally, the double mutant exhibited almost the same growth as *glo3-R59K* mutant cells (Fig. 3F). These results suggest that function of Gcs1p is not critical for Ste2p recruitment to the plasma membrane.

3.4. The GAP domain and the BoCCS region play important roles in Ste2p recycling.

Similar to the effect on Ste2-GFP localization, decreased binding of α-factor was also observed in *glo3-R59K* cells (Fig. 3E), although the effects for both were only partial, suggesting a requirement for a GAP-independent function of Glo3p during Ste2p transport. To examine this possibility we created Glo3 mutants that deleted the GAP domain (ΔGAP) or the binding of coatomer, cargo and SNARE region (ΔBoCCS) (Fig. 4A). As described previously, the GAP domain was required for growth at an elevated temperature (37^{o}C) (Fig. 4B) [31]. We first investigated the effect of these deletions on Ste2p localization. In cells expressing Glo3ΔGAP, the localization of Ste2p was partly shifted to the intracellular compartments (Fig. 4C). Cells expressing Glo3ΔBoCCS also exhibited partially decreased Ste2p localization at the plasma membrane (Fig. 4C). We further compared ^{35}S-labeled α-factor binding among these

mutant cells. Consistent with Ste2p localization, cells expressing Glo3ΔGAP or Glo3ΔBoCCS exhibited a partial defect in the binding of α-factor (Fig. 4D). These results clearly indicate that both the BoCCS region and the GAP domain play important roles in Ste2p recycling.

3.5. Effect of *GLO3* deletion on protein transport from the Golgi to the vacuole

As *glo3*Δ cells have been reported to impair the transport of CPY (carboxypeptidase Y) from the endoplasmic reticulum (ER) to the vacuole [17], we next investigated the effects of *GLO3* deletion on vesicular trafficking pathways from the Golgi to the vacuole. To examine the defect in the VPS pathway quantitatively, we examined the secretion of CPY using a colony blot assay. In wild-type cells, CPY was efficiently sorted to the vacuole and therefore was not secreted, whereas a significant amount of CPY was secreted in mutant cells lacking *VPS27*, which is a class E *VPS* gene important for vesicle transport via the CPY pathway (Fig. 5A). Consistent with previous studies [17, 21], *glo3*Δ cells exhibited a small CPY secretion phenotype, whereas *gcs1*Δ, *age1*Δ, and *gts1*Δ cells did not secrete any detectable CPY (Fig. 5A). The secretion observed in *glo3*Δ cells was much less than that in *vps27*Δ cells. *age2*Δ cells also exhibited a mild CPY secretion phenotype (Fig. 5A), consistent with a previous study showing that Age2p and Gcs1p have overlapping functions for TGN transport, including CPY transport [21]. We also examined the effects of the deletion of these genes on the transport of Pep4-GFP from the ER to the vacuole through the VPS pathway. No obvious defect in the transport of Pep4-GFP to the vacuole was observed

in any of the GAP mutants, whereas aberrant accumulation of Pep4-GFP in multiple endosomal compartments was observed in *vps21*Δ cells, which were previously shown to have severe defects in the VPS pathway (Fig. 5B) [32]. These results suggest that *glo3*Δ cells have subtly defective transport from the Golgi to the vacuole.

3.6. Localization of Glo3p at the Golgi apparatus and the effect of deleting the *GLO3* gene on Arf protein localization

Glo3p has been considered to mediate vesicular transport between the ER and the Golgi, but the precise location of Glo3p function has not been clarified. We therefore tagged endogenous Glo3p with GFP, and examined its localization in living cells; the functionality of the GFP-Glo3p was confirmed by testing its ability to complement the growth phenotype of *glo3*Δ cells (Fig. 6A). GFP-Glo3 was detected in several punctate structures throughout the cytoplasm (Fig. 6B). We next compared the localization of GFP-Glo3 with mCherry-tagged markers localizing to different compartments of the Golgi apparatus. A high degree of colocalization of GFP-Glo3 and mCherry-tagged Vrg4p (~52.7%), a marker for *cis*-Golgi, or Mnn5p (~55.3%), a marker for *medial*-Golgi, indicated that the majority of Glo3p was localized at the *cis*-to-*medial*-Golgi compartments (Fig. 6B), consistent with the previous observation that Glo3p mediates retrograde vesicular transport from the *cis*-Golgi to the ER [17]. Glo3p also partly colocalized with Sec7- or Kex2-mCherry (~12.5% or ~16.0%, respectively), markers for the TGN (Fig. 6B, C). On the other hand, Glo3p rarely colocalized with the mitochondria labeled by mitotracker (<3%) which was used as a

negative control (Fig. 6B). Thus, Glo3p is likely to be localized throughout the Golgi apparatus. In yeast, three ARFs have been identified [8, 11, 33], and two of them, Arf1p and Arf2p, are believed to participate in vesicular trafficking in the Golgi and have been localized to the Golgi [34]. In contrast, Arf3p, whose sequence is 60% identical to that of mammalian ARF6, is localized to the plasma membrane and implicated in endocytic internalization [30]. As expected, Glo3p was well colocalized with Arf1p (~63.3%) and Arf2p (~56.7%) (Fig. 6B and 6C).

Since it has been established that Glo3p functions as a GAP for yeast ARFs [17, 20] and that GTP-bound active ARFs associate with membranes and dissociate when GTP is hydrolyzed to GDP, we next examined whether deletion of *GLO3* could affect the localization of Arf1p or Arf2p. We first confirmed the functionality of the GFP-tagged Arf1p by demonstrating its ability to complement the growth phenotype of *arf1*Δ cells (Fig. 6A, right panel). Arf2p is reported to be expressed ~10-fold lower than Arf1p and *arf2*Δ cells display no growth phenotype, thus we did not test the functionality of the Arf2-GFP [8]. In wild-type cells, ~49.2% of Arf1-GFP and ~59.9% of Arf2-GFP were localized to Sec7p-residing *trans*-Golgi compartments; the deletion of *GLO3* led to an increased association of these proteins with the *trans*-Golgi compartments (~63.0% and ~69.8%, respectively) (Fig. 7A and 7C). In contrast, in wild-type cells ~60.8% of Arf1p and ~55.6% of Arf2p were localized to the *cis*-Golgi compartments labeled by Vrg4-GFP, and their localization there was decreased in *glo3*Δ cells (~34.2% or 30.0%) (Fig. 7B and 7C). Again, little localization of Arf1p or Arf2p was observed in the mitochondria (<3%) (Fig. 7D). It is noteworthy that in *glo3*Δ cells

the Golgi compartments labeled by both Arf1-GFP and Sec7-mCherry tended to be slightly enlarged (Fig. 7E) and their average number was remarkably decreased (Fig. 7F). These results suggest that in *GLO3*-disrupted cells increased levels of GTP-locked Arf1p, which could stably associate with the Golgi membranes, might affect maturation of the Golgi cisternae, resulting in a defect of Arf1p-mediated transport from the Golgi to the plasma membrane.

3.7. Glo3p is required for Snc1p transport from the TGN to the plasma membrane

To further address the specific role of Glo3p in protein transport from the Golgi to the plasma membrane, we examined the effect of *glo3*Δ on trafficking of GFP-Snc1p, an exocytic v-SNARE that is endocytosed, transiently localized to early endosomes, and recycled back to the plasma membrane via the *trans*-Golgi compartment [35, 36]. It has been shown that mutations affecting endosome-mediated trafficking often cause mis-localization of Snc1p from the plasma membrane to the endosomal or vacuolar compartments [35-37]. In wild-type cells, GFP-Snc1p was localized at the plasma membrane with some punctate staining of internal structures (Fig. 8A and 8B), as shown in previous studies. Intriguingly, in *glo3*Δ cells, localization of GFP-Snc1 was partly shifted to intracellular compartments, in contrast to its predominant localization at the plasma membrane in *gcs1*Δ cells (Fig. 8A). Quantitative analysis showed that in wild type 100% of cells showed GFP-Snc1 at the plasma membrane but in *glo3*Δ cells only 62% did, with ~38% of *glo3*Δ cells exhibiting GFP-Snc1 predominantly in intracellular compartments (Fig. 8B). These intracellular

structures were significantly co-localized with Sec7, a *trans*-Golgi marker (Fig. 8C and 8D). This observation implies that *glo3*Δ cells were defective in the TGN-to-plasma membrane pathway, but not in the early endosome-to-TGN transport pathway. We next examined which domain of Glo3 was required for Snc1p transport from the TGN to the plasma membrane. A significant change in Snc1p localization was observed only in the ΔGAP mutant, suggesting that this domain is particularly important in Glo3 for Snc1p transport (Figure 8E and 8F). To further characterize the GFP-Snc1 localization defect in *glo3*Δ cells, we used a GFP-fused Snc1(en-) mutant, which contains two mutations, V40A and M43A, that interfere with endocytosis and cause GFP-Snc1 to accumulate on the plasma membrane in wild type cells (Fig. 8G) [35]. As shown in Fig. 8E, we observed that GFP-Snc1(en-) is also localized to the plasma membrane in *glo3*Δ cells. Quantitative analysis showed that in *glo3*Δ cell 100% of cells showed GFP-Snc1(en-) at the plasma membrane. These results, taken together, suggest that *glo3*Δ cells were defective in the TGN-to-plasma membrane pathway, but that the pathway was not completely disrupted.

3.8. The *glo3*Δ cell is defective in the retrieval pathway from the late endosome to the TGN

The observation that Ste2p has the ability to get to the cell surface but accumulates in the vacuole in *glo3*Δ cells suggests that *glo3*Δ cells might have a defect in transport from the endosome to the TGN. Thus, we next investigated the late endosomal retrieval pathway in *glo3*Δ cells. Kex2p is a pheromone-processing protease

residing at the TGN which is transported to the late endosome and recycled back to the TGN in a retromer-dependent manner [35, 38]. Kex2-GFP is localized to punctate structures in wild-type cells, whereas deletion of *GLO3* caused mis-localization of Kex2p to the vacuole (Fig. 9A). Taken together with the Snc1p localization studies, these results suggest that *glo3*Δ cells were defective in the late endosome-to-TGN transport pathway, but not in the early endosome-to-TGN transport pathway. To confirm this idea, we further examined the localization of the t-SNARE Tlg1p, which is recycled between early endosomes and the TGN [35, 39]. As expected, the localization of Tlg1-GFP to internal punctate structures was normal in *glo3*Δ cells (Fig. 9B). Finally, to examine whether Glo3p function is generally required for cell surface protein recycling, we used the yeast general amino acid permease Gap1p that is known to be recycled to the plasma membrane via the TGN after endocytic internalization [40]. Similarly to Ste2p, ~96% of wild-type cells exhibited localization of Gap1-GFP at the plasma membrane as well as the vacuole, but the cell surface localization was significantly decreased in the *glo3*Δ cells (Fig. 9C), suggesting a general role for Glo3p in cell surface protein recycling.

4. Discussion

In this study, we probed the pathway of endocytosis from the plasma membrane to the vacuole in 25 GAP deletion mutants and found that the *glo3*Δ mutant exhibited defects in the internalization of fluorescently labeled α-factor. Interestingly,

quantitative analysis revealed that these *glo3*Δ mutant cells or ones expressing a GAP activity-deficient form of Glo3p had a defect in α-factor binding to the cell surface. This result could be explained by our finding that, in *glo3*Δ cells, the α-factor receptor, Ste2p, was sorted to the vacuole even when no α-factor was present.

While it is known that upon binding α-factor, Ste2p is triggered to undergo transport through the endocytic pathway to the vacuole [23, 41, 42], it has not been well characterized if Ste2p in the absence of α-factor is recycled back to the plasma membrane, much less how this might occur. We believe our results can shed some light on this question. We showed that Ste2p has the ability to get to the cell surface in *glo3*Δ cells although the transport is less efficient than that in wild-type cells. We also demonstrated that *glo3*Δ cells have a defect in transport back to the TGN from the late but not the early endosome; in *glo3*Δ cells the late endosomal Kex2p is mis-sorted to the vacuole but the early endosomal Snc1p and Tlg1p are transported normally to the TGN (Fig. 10A and 10B). From these observations, we propose that, in *glo3*Δ cells, newly synthesized Ste2p is first transported to the plasma membrane, then constitutively endocytosed, and finally sorted to the vacuole without being recycled, resulting in a decrease of cell surface Ste2p (Fig. 10B); Gap1p is also mislocalized to the vacuole in a similar manner (Fig. 10A and 10B). In wild-type cells, we propose that Ste2p is also constitutively endocytosed, but is retrieved to the TGN from the late endosome and shuttled again back to the cell surface (Fig. 10A).

In this study we provide evidence that a GAP-dependent and GAP-independent function of Glo3p are required for this Ste2p recycling. We find that

both *glo3-R59K* and *glo3ΔGAP* mutants exhibited partial defects in the binding of α-factor. This GAP independent function may be related to previous findings that Arf-GAPs are also important regulators of vesicle formation and fusion [4, 52]. At the time of vesicle budding, the Arf-GAPs Glo3p and Gcs1p are recruited to the donor membrane and form a priming complex, with Arf1p, coatomers, and cargos [52]. Simultaneously, Glo3p and Gcs1p bind to and induce a conformational change in the v-SNAREs involved in ER-Golgi and post-Golgi trafficking [53, 54]. Furthermore at the time of vesicle fusion, these Arf-GAPs promote v- and t-SNARE complex formation and also recruit Sec18p, the yeast NSF [55]. Such functions could require a separate domain than that utilized for the GAP function; interestingly, the *glo3ΔBoCCS* mutant also exhibited a partial defect in the binding of α-factor and mis-localization of Ste2p in the vacuole. Thus, a GAP–independent function is required for late endosome-to-Golgi transport, likely a Glo3-mediated formation of priming complex and/or SNARE.

Yeast has six Arf-GAP proteins [17, 19, 21, 46], but it has not been clarified which GAP(s) is implicated in vesicle transport from the TGN to the plasma membrane. Previous studies have shown that Glo3p is required for the secretion of invertase [17]. As discussed above Glo3p plays a direct role in coat assembly, interacting with SNARE proteins and inducing a conformational change that allows recruitment of Arf1p and coatomer to the SNAREs [48]; in fact overexpression of Glo3p suppresses a loss-of-function allele of *ARF1* [17, 18, 20]. The TGN to plasma membrane transport defects observed in the *glo3Δ* mutant are probably due to this role in Arf1 recruitment

and coat assembly on transport vesicles. In support of this idea, *arf1-11 arf2*Δ cells were shown to have defects in general (bulk) secretion of proteins, including invertase [10].

The GAP dependent function of Glo3p seems to provide the main role for the localization of the exocytic v-SNARE, Snc1p. While Ste2p was mis-localized to the vacuole both in the *glo3*Δ*GAP* and *glo3*Δ*BoCCS* domain mutants (Fig. 4D), Snc1p was partly shifted to intracellular compartments in the *glo3*Δ*GAP* mutant, but no such mis-localization was observed in the *glo3*Δ*BoCCS* mutant (Fig 8G). This suggests that Snc1p's defective transport from the Golgi to the plasma membrane might be principally due to the perturbation of Golgi function caused by GTP-locked Arf1/2p.

Our results initially appear to contrast with those of a recent study on another Arf GAP in plants. Min et al. reported that in the absence of either of two Glo3-type Arf GAPs, AGD8 and AGD9, Arf1-GDP is not recruited as efficiently to the Golgi apparatus in Arabidopsis [49]. Our results in *S. cerevisiae* demonstrate that in the absence of Glo3p, Arf1p and Arf2p increased their association with *trans*-Golgi compartments. We propose however, that in both cases the GTP-bound forms cannot be extracted as efficiently from the organellar membrane with which they associate. The delay in Arf1p recruitment to the Golgi observed in cells with decreased levels of AGD8/AGD9 might be caused by a reduction in the pool of Arf1p in the cytosol due to an increase in static Arf1p at the Golgi membrane: RNA interference of AGD8/AGD9 would increase the GTP-bound form of Arf1p that cannot dissociate from the Golgi membrane, resulting in a decrease of cytosolic Arf1p.

We have proposed that the *glo3*Δ mutant has a defect in α-factor binding due

to defects in Ste2p recycling to the plasma membrane, but why A594-α-factor internalization is delayed (Fig. 10B) is unclear. After binding α-factor, Ste2p is rapidly phosphorylated at the C-terminal region by Yck1p and Yck2p; this leads to Ste2p ubiquitination, which facilitates recruitment of the receptor to clathrin-coated pits [23, 43]. Therefore, one possible explanation for the defective α-factor internalization in *glo3Δ* cells could be that the lower expression of Ste2p at the plasma membrane reduces the probability of Ste2p encountering the kinases and ubiquitinating enzymes whose actions promote endocytosis. Decreased expression of Ste2p at the plasma membrane might also affect the dimerization efficiency of Ste2p. Since it has been demonstrated that Ste2p is internalized as a dimer/oligomer complex [44, 45], and that oligomerization-defective mutants can bind α-factor but their signaling is impaired [46], defective dimerization might delay the internalization of α-factor.

It still remains elusive how membrane proteins, such as Ste2p, are transported from the TGN to the cell surface. In yeast there are at least two routes, which can be separated based on the densities of the vesicles they utilize and are therefore classified as light- and heavy-density secretory vesicle pathways (LDSV and HDSV) [56, 57]. These two vesicle types transport different cargo proteins; LDSVs are responsible for transporting integral plasma membrane proteins, such as Pma1p, Hxt2p, and Gas1p, as well as a variety of cell wall proteins, whereas HDSVs transport the periplasmic enzymes invertase and acid phosphatase [56, 58]. Recent studies have revealed that some of the cargos transported by LDSVs require the exomer complex for their exit from the TGN [59]. The exomer is an Arf1 GTPase-dependent protein complex required

for trafficking of specific cargo proteins from the TGN to the plasma membrane [13-15]. Intriguingly, both of the exomer subunits, Chs5p and Chs6p, bind preferentially to the active form of Arf1p [13]. Furthermore, *chs5*Δ cells show a strong mating defect [60] suggesting that Ste2p transport from the TGN to the plasma membrane might be mediated by the Arf1 GTPase-dependent exomer complex.

Acknowledgements

We thank Dr. Hugh Pelham for kindly providing the GFP-Snc1(en-) plasmid. This work was supported by the Japan Society for the promotion of Science for J.Y.T., and the Novartis Foundation (Japan), the Mitsubishi foundation, the Naito Foundation, the Mochida Memorial Foundation for Medical and Pharmaceutical Research, the Futaba Electronics Memorial Foundation, the Astellas Foundation for Research on Metabolic Disorders, the Hamaguchi Foundation for the Advancement of Biochemistry, the Takeda Science Foundation, and the Kurata Memorial Hitachi Science and Technology Foundation, to J.T.

Figure Legends

Fig. 1. Effect of deleting Arf-, Rab-, and Rho-GAP genes on the endocytic pathway. (**A**) Wild-type and *end3*Δ cells were labeled with A594-α-factor as described in the Materials and Methods. The cells were observed by fluorescence microscopy and different interference contrast (DIC) at 15 min after washing out unbound A594-α-factor and warming the cells to 25°C. Scale bar, 2.5 μm. (**B-D**) Cells depleted of Arf-GAPs (B), Rab-GAPs (C), or Rho-GAPs (D) were treated with A594-α-factor and observed as described in (A). The boxed names denote strains that exhibit abnormal A594-α-factor localization. Scale bars, 2.5 μm. (**E**) Quantification of localization of A594-α-factor in wild-type and mutant cells. The bar graphs represent the percentages of cells exhibiting A594-α-factor localized at the vacuole only at 30 min after internalization. Data show mean from at least two experiments, with >50 cells counted for each strain per experiment.

Fig. 2. Glo3p and Gts1p do not have overlapping function in endocytic internalization. (**A**) Wild-type, *glo3*Δ, *gts1*Δ or *glo3*Δ *gts1*Δ cells were treated with A594-α-factor, and the images were acquired 15 and 30 min after washing out unbound A594-α-factor and warming the cell to 25°C. Scale bar, 2.5 μm. (**B**) Quantification of localization of A594-α-factor in wild-type and mutant cells at 15 min after internalization. The bar graphs represent the percentages of cells exhibiting A594-α-factor localized at the vacuole only (red), the endosome and vacuole (yellow), or the plasma membrane (blue) at 15 min after internalization. Data show mean ± standard deviation (SD) from at least

three experiments, with >100 cells counted for each strain per experiment. (**C**) Radiolabeled α-factor internalization assays performed on the indicated strains at 25°C. Each curve represents the average of three independent experiments, and error bars indicate the SD at each time point. (**D**) The amount (cpm) of membrane-bound radiolabeled α-factor was calculated from the assay shown in (C). The amount was calculated by subtracting ^{35}S signal of acid washed cells (internal ^{35}S signal) from ^{35}S signal of cells washed by pH 6 buffer (total ^{35}S signal). Error bars indicate the SD from at least three experiments. ***, *p* value < 0.005.

Fig. 3. Localization of α-factor receptor, Ste2p, in the *glo3*Δ mutants and relative amount of α-factor bound to the Arf-GAP mutants. (**A**) Cells expressing Ste2-GFP were grown to early to mid-logarithmic phase in YPD medium at 25°C and observed by fluorescence microscopy and DIC. Scale bar, 2.5 μm. (**B**) Quantification of localization of Ste2-GFP at the plasma membrane (PM). Localization of Ste2-GFP at the PM was quantified as percentage of cells in which fluorescent intensity of Ste2-GFP at the PM is higher than that at the cytosol. Data show mean ± SD from at least three experiments, with >100 cells counted for each strain per experiment. (**C**) Localization of Ste2-GFP and mCherry-tagged Pep4p in wild-type and *glo3*Δ cells. Merged images of GFP and mCherry channels are also shown in the rightmost column. Cells expressing Ste2-GFP and Pep4-mCherry were grown and observed as described in (A). Scale bar, 2.5 μm. (**D**) Localization of Ste2Δ300-GFP in wild-type or *glo3*Δ cell. Cells expressing Ste2Δ300-GFP were labeled with A594-α-factor as described in the Methods. The

images were acquired simultaneously after washing out unbound A594-α-factor. Scale bar, 2.5 μm. (**E**) Relative amount of α-factor bound to wild-type and Arf-GAP mutant cells. Cells were grown to early to mid-logarithmic phase in YPD medium at 25°C, briefly centrifuged, and resuspended in 50 μl synthetic media (SM) with 1% (w/v) BSA and radiolabeled α-factor. After incubation on ice for 2 h, cells were washed with ice-cold SM and measured for their radioactivity. Error bars represent the SD from at least three experiments. ***, *p* value < 0.005. (**F**) The *glo3-R59K gcs1*Δ double mutant does not exhibit an additive growth defect. A dilution series of cells were plated on YPD medium and incubated at 30°C.

Fig. 4. The GAP domain and the BoCCS region have important roles in Ste2p recycling. (**A**) Schematic diagram of Glo3 deletion mutants. GAP domain, BoCCS, and GRM regions are indicated. (**B**) Plates showing the growth phenotype of Glo3 deletion mutants. A dilution series of cells was plated on SD-URA plate and incubated at 37°C. (C) Localization of Ste2p, in Glo3 deletion mutants. Cells expressing Ste2-GFP were grown to early to mid-logarithmic phase at 25°C and observed by fluorescence microscopy and DIC. Scale bar, 2.5 μm. (**D**) The relative amount of α-factor bound to Glo3 deletion mutants was analyzed as described in Fig. 3E. ***, *p* value < 0.005.

Fig. 5. Effect on the VPS pathway of deleting Arf-GAP family genes. (**A**) CPY sorting analysis. The indicated strains were grown on a YPD plate and then replica-plated onto anitrocellulose filter. The filter was washed with PBS buffer, and secreted CPY was

detected using anti-CPY antibody. The histogram in the right panel represents the relative intensities of CPY secretion quantified by chemiluminescence signals. Data show mean ± SD from three experiments. (**B**) Transport of GFP-tagged Pep4p in wild-type, *vps21*Δ, or Arf-GAP mutant cells. Cells expressing Pep4-GFP were grown to early to mid-logarithmic phase in YPD medium at 25°C and observed by fluorescence microscopy and DIC. Scale bar, 2.5 μm.

Fig. 6. The functionality and localization of GFP-tagged Glo3p. (**A**) Functionality of GFP-tagged Glo3p and Arf1p. A dilution series of cells was plated on YPD medium and incubated at 39°C. (**B**) Localization of GFP-Glo3 and mCherry-tagged proteins in living cells. Merged images of GFP and mCherry channels are also shown in the right panels. Wild-type cells expressing GFP-Glo3 and mCherry-tagged proteins were grown to early to mid-logarithmic phase in YPD medium at 25°C and observed by fluorescence microscopy. Each image pair was acquired simultaneously. Arrowheads indicate examples of colocalization. Scale bar, 2.5 μm. (**C**) Quantification of colocalization of Glo3p and Golgi markers in wild-type cells. The histogram represents the percentage of GFP-Glo3 labeled compartments colocalizing with indicated organellar markers. Co-localization was evaluated by visual inspection of signal overlap on merged RGB images. In each experiment n = 100 GFP-Glo3 labeled compartments were counted for each marker protein. Error bars indicate the SD from at least three independent experiments.

Fig. 7. Localization of Arf1 and Arf2 proteins in wild-type and *glo3*Δ cells. (**A**, **B**) Localization of Arf proteins and Sec7-mCherry (A) or Vrg4-GFP (B) in wild-type and *glo3*Δ cells. Merged images of GFP and mCherry channels are shown in the lower panels. Each image pair was acquired simultaneously. Arrowheads indicate examples of colocalization. Scale bars, 2.5 μm. (**C**) Quantification of the colocalization of Arf proteins and Sec7p or Vrg4p in wild-type and *glo3*Δ cells. The histogram represents the percentage of Arf1p or Arf2p labeled compartments colocalizing with Sec7-mCherry or Vrg4-GFP. Co-localization was evaluated by visual inspection of signal overlap on merged RGB images. In each experiment $n = 100$ Arf1p or Arf2p labeled compartments were counted for each marker protein. Error bars indicate the SD from at least three independent experiments. *, p value <0.05. (**D**) Localization of Arf proteins and mitotracker in wild-type and *glo3*Δ cells. Scale bar, 2.5 μm. (**E**) Maximum intensity projections of Z stacks of wild-type and *glo3*Δ cells labeled with Arf1-GFP and Sec7-mCherry. The Z series was acquired through the entire cell at 0.3 μm intervals. Dotted lines represent the outline of cells. Arrowheads indicate examples of colocalization. Scale bar, 2.5 μm. (**F**) Quantification of Arf1-GFP puncta per cell ($n = 50$ cells for each strain). ***, p value < 0.005. Charts show box plots of the data. The line indicates the median, the edges of the box indicate the 25 and 75% percentiles, and the whiskers extend to the extremes of the data.

Fig. 8. Glo3p is required for Snc1p recycling to the plasma membrane. (**A**) Localization of GFP-Snc1 in wild-type, *glo3*Δ, and *gcs1*Δ cells. Cells expressing GFP-Snc1 were

grown to early to mid-logarithmic phase in YPD medium at 25^{o}C and observed by fluorescence microscopy and DIC. Scale bar, 2.5 μm. (**B**) Quantification of localization of GFP-Snc1 at the plasma membrane (PM). The localization of Snc1-GFP at the PM was quantified as the percentage of cells in which the fluorescent intensity of Snc1-GFP at the PM is higher than that in the cytosol. Data show mean ± SD from at least three experiments, with >100 cells counted for each strain per experiment. ***, *p* value < 0.005. (**C**) Localization of GFP-Snc1 and Sec7-mCherry in wild-type or *glo3*Δ cells. Cells expressing GFP-Snc1 and Sec7-mCherry were grown and observed as described in (A). Scale bar, 2.5 μm. (**D**) Quantification of colocalization of GFP-Snc1 and Sec7-mCherry in wild-type or *glo3*Δ cells. Co-localization was evaluated by visual inspection of signal overlap on merged RGB images. The histogram represents the percentage of Snc1-GFP labeled compartments colocalizing with Sec7-mCherry. In each experiment *n* = 100 Snc1-GFP labeled endosomes were counted. Error bars indicate the SD from at least three independent experiments. **P <0.01. (**E, F**) Localization of Snc1-GFP was analyzed as described in (A and B). Scale bar, 2.5 μm. ***, *p* value < 0.005. (**G**) Localization of GFP-Snc1(en-) in wild-type and *glo3*Δ cells. Cells expressing GFP-Snc1(en-) were grown to early to mid-logarithmic phase at 25^{o}C and observed by fluorescence microscopy and DIC. Scale bar, 2.5 μm.

Fig. 9. *glo3*Δ cells exhibit mis-localization of Kex2p, Gap1p, but not Tlg1p. (**A**) Localization of Kex2-GFP in wild-type and *glo3*Δ cells. Cells expressing Kex2-GFP were grown to early to mid-logarithmic phase in YPD medium at 25^{o}C and observed by

fluorescence microscopy and DIC. Right bar graphs represent the percentages of cells exhibiting Kex2-GFP localization at the vacuole. Data show mean ± SD from at least three experiments, with >50 cells counted for each strain per experiment. (**B**) Localization of GFP-Tlg1 in wild-type and *glo3*Δ cells. Cells expressing GFP-Tlg1 and Sec7-mCherry were grown and observed as described in (A). The histogram represents the percentages of GFP-Tlg1 labeled compartments colocalizing with Sec7-mCherry. Data show mean ± SD from at least three experiments, with >50 cells counted for each strain per experiment. (**C**) Localization of Gap1-GFP in wild-type and *glo3*Δ cells. Cells expressing Gap1-GFP were grown to early to mid-logarithmic phase in synthetic medium supplemented with 2% glucose and low levels of amino acids at 25^{o}C. The histogram represents the percentages of cells exhibiting Gap1-GFP localization at the plasma membrane. Data show mean ± SD from at least three experiments, with >50 cells counted for each strain per experiment. Scale bars, 2.5 μm.

Fig. 10. Model for the localization and function of Glo3p. Glo3p localizes in the Golgi apparatus and regulates protein recycling and secretory pathways. In *glo3*Δ cells, transport from the late endosome to the TGN is severely inhibited, resulting in mis-localization of Ste2p, Gap1p and Kex2 to the vacuole. *glo3*Δ cells also have defects in transport from the TGN to the plasma membrane and in Ste2 internalization. See details in the text. Red T bars indicate the steps which show defects in the absence of Glo3p.

References

[1] J. Colicelli, Human RAS superfamily proteins and related GTPases, Sci STKE, 2004 (2004) RE13.

[2] A.B. Jaffe, A. Hall, Rho GTPases: biochemistry and biology, Annu Rev Cell Dev Biol, 21 (2005) 247-269.

[3] T. Kirchhausen, Three ways to make a vesicle, Nature reviews. Molecular cell biology, 1 (2000) 187-198.

[4] A. Spang, ARF1 regulatory factors and COPI vesicle formation, Curr Opin Cell Biol, 14 (2002) 423-427.

[5] Z. Nie, D.S. Hirsch, P.A. Randazzo, Arf and its many interactors, Curr Opin Cell Biol, 15 (2003) 396-404.

[6] M. Tsuchiya, S.R. Price, S.C. Tsai, J. Moss, M. Vaughan, Molecular identification of ADP-ribosylation factor mRNAs and their expression in mammalian cells, J Biol Chem, 266 (1991) 2772-2777.

[7] C. D'Souza-Schorey, P. Chavrier, ARF proteins: roles in membrane traffic and beyond, Nature reviews. Molecular cell biology, 7 (2006) 347-358.

[8] T. Stearns, R.A. Kahn, D. Botstein, M.A. Hoyt, ADP ribosylation factor is an essential protein in Saccharomyces cerevisiae and is encoded by two genes, Mol Cell Biol, 10 (1990) 6690-6699.

[9] A.K. Gillingham, S. Munro, The small G proteins of the Arf family and their regulators, Annu Rev Cell Dev Biol, 23 (2007) 579-611.

[10] N. Yahara, T. Ueda, K. Sato, A. Nakano, Multiple roles of Arf1 GTPase in the yeast exocytic and endocytic pathways, Mol Biol Cell, 12 (2001) 221-238.

[11] T. Stearns, M.C. Willingham, D. Botstein, R.A. Kahn, ADP-ribosylation factor is functionally and physically associated with the Golgi complex, Proc Natl Acad Sci U S A, 87 (1990) 1238-1242.

[12] S. Sanchatjate, R. Schekman, Chs5/6 complex: a multiprotein complex that interacts with and conveys chitin synthase III from the trans-Golgi network to the cell surface, Mol Biol Cell, 17 (2006) 4157-4166.

[13] M. Trautwein, C. Schindler, R. Gauss, J. Dengjel, E. Hartmann, A. Spang, Arf1p, Chs5p and the ChAPs are required for export of specialized cargo from the Golgi, Embo J, 25 (2006) 943-954.

[14] C.W. Wang, S. Hamamoto, L. Orci, R. Schekman, Exomer: A coat complex for

transport of select membrane proteins from the trans-Golgi network to the plasma membrane in yeast, J Cell Biol, 174 (2006) 973-983.

[15] J.E. Paczkowski, B.C. Richardson, A.M. Strassner, J.C. Fromme, The exomer cargo adaptor structure reveals a novel GTPase-binding domain, Embo J, 31 (2012) 4191-4203.

[16] P.P. Poon, X. Wang, M. Rotman, I. Huber, E. Cukierman, D. Cassel, R.A. Singer, G.C. Johnston, Saccharomyces cerevisiae Gcs1 is an ADP-ribosylation factor GTPase-activating protein, Proc Natl Acad Sci U S A, 93 (1996) 10074-10077.

[17] P.P. Poon, D. Cassel, A. Spang, M. Rotman, E. Pick, R.A. Singer, G.C. Johnston, Retrograde transport from the yeast Golgi is mediated by two ARF GAP proteins with overlapping function, Embo J, 18 (1999) 555-564.

[18] C.J. Zhang, M.M. Cavenagh, R.A. Kahn, A family of Arf effectors defined as suppressors of the loss of Arf function in the yeast Saccharomyces cerevisiae, J Biol Chem, 273 (1998) 19792-19796.

[19] C.J. Zhang, J.B. Bowzard, A. Anido, R.A. Kahn, Four ARF GAPs in Saccharomyces cerevisiae have both overlapping and distinct functions, Yeast, 20 (2003) 315-330.

[20] S.M. Lewis, P.P. Poon, R.A. Singer, G.C. Johnston, A. Spang, The ArfGAP Glo3 is required for the generation of COPI vesicles, Mol Biol Cell, 15 (2004) 4064-4072.

[21] P.P. Poon, S.F. Nothwehr, R.A. Singer, G.C. Johnston, The Gcs1 and Age2 ArfGAP proteins provide overlapping essential function for transport from the yeast trans-Golgi network, J Cell Biol, 155 (2001) 1239-1250.

[22] J.Y. Toshima, J. Toshima, M. Kaksonen, A.C. Martin, D.S. King, D.G. Drubin, Spatial dynamics of receptor-mediated endocytic trafficking in budding yeast revealed by using fluorescent alpha-factor derivatives, Proc Natl Acad Sci U S A, 103 (2006) 5793-5798.

[23] J.Y. Toshima, J.I. Nakanishi, K. Mizuno, J. Toshima, D.G. Drubin, Requirements for Recruitment of a G Protein-coupled Receptor to Clathrin-coated Pits in Budding Yeast, Mol Biol Cell, (2009).

[24] M.S. Longtine, A. McKenzie, 3rd, D.J. Demarini, N.G. Shah, A. Wach, A. Brachat, P. Philippsen, J.R. Pringle, Additional modules for versatile and economical PCR-based gene deletion and modification in Saccharomyces cerevisiae, Yeast, 14 (1998) 953-961.

[25] J. Toshima, J.Y. Toshima, A.C. Martin, D.G. Drubin, Phosphoregulation of Arp2/3-dependent actin assembly during receptor-mediated endocytosis, Nat Cell Biol, 7 (2005) 246-254.

[26] A. Kojima, J.Y. Toshima, C. Kanno, C. Kawata, J. Toshima, Localization and functional requirement of yeast Na(+)/H(+) exchanger, Nhx1p, in the endocytic and protein recycling pathway, Biochim Biophys Acta, 1823 (2012) 534-543.

[27] H.Y. Tang, A. Munn, M. Cai, EH domain proteins Pan1p and End3p are components of a complex that plays a dual role in organization of the cortical actin cytoskeleton and endocytosis in Saccharomyces cerevisiae, Mol Cell Biol, 17 (1997) 4294-4304.

[28] E.S. Seeley, M. Kato, N. Margolis, W. Wickner, G. Eitzen, Genomic analysis of homotypic vacuole fusion, Mol Biol Cell, 13 (2002) 782-794.

[29] R. Smaczynska-de, II, R. Costa, K.R. Ayscough, Yeast Arf3p modulates plasma membrane PtdIns(4,5)P2 levels to facilitate endocytosis, Traffic, 9 (2008) 559-573.

[30] C.P. Toret, L. Lee, M. Sekiya-Kawasaki, D.G. Drubin, Multiple pathways regulate endocytic coat disassembly in Saccharomyces cerevisiae for optimal downstream trafficking, Traffic, 9 (2008) 848-859.

[31] C. Schindler, F. Rodriguez, P.P. Poon, R.A. Singer, G.C. Johnston, A. Spang, The GAP domain and the SNARE, coatomer and cargo interaction region of the ArfGAP2/3 Glo3 are sufficient for Glo3 function, Traffic, 10 (2009) 1362-1375.

[32] B. Singer-Kruger, H. Stenmark, A. Dusterhoft, P. Philippsen, J.S. Yoo, D. Gallwitz, M. Zerial, Role of three rab5-like GTPases, Ypt51p, Ypt52p, and Ypt53p, in the endocytic and vacuolar protein sorting pathways of yeast, J Cell Biol, 125 (1994) 283-298.

[33] F.J. Lee, L.A. Stevens, Y.L. Kao, J. Moss, M. Vaughan, Characterization of a glucose-repressible ADP-ribosylation factor 3 (ARF3) from Saccharomyces cerevisiae, J Biol Chem, 269 (1994) 20931-20937.

[34] A.K. Gillingham, A.H. Tong, C. Boone, S. Munro, The GTPase Arf1p and the ER to Golgi cargo receptor Erv14p cooperate to recruit the golgin Rud3p to the cis-Golgi, J Cell Biol, 167 (2004) 281-292.

[35] M.J. Lewis, B.J. Nichols, C. Prescianotto-Baschong, H. Riezman, H.R. Pelham, Specific retrieval of the exocytic SNARE Snc1p from early yeast endosomes, Mol Biol Cell, 11 (2000) 23-38.

[36] J.M. Galan, A. Wiederkehr, J.H. Seol, R. Haguenauer-Tsapis, R.J. Deshaies, H. Riezman, M. Peter, Skp1p and the F-box protein Rcy1p form a non-SCF complex involved in recycling of the SNARE Snc1p in yeast, Mol Cell Biol, 21 (2001) 3105-3117.

[37] F. Reggiori, C.W. Wang, P.E. Stromhaug, T. Shintani, D.J. Klionsky, Vps51 is part of the yeast Vps fifty-three tethering complex essential for retrograde traffic from the early endosome and Cvt vesicle completion, J Biol Chem, 278 (2003) 5009-5020.

[38] M.N. Seaman, J.M. McCaffery, S.D. Emr, A membrane coat complex essential for endosome-to-Golgi retrograde transport in yeast, J Cell Biol, 142 (1998) 665-681.

[39] J.C. Holthuis, B.J. Nichols, H.R. Pelham, The syntaxin Tlg1p mediates trafficking of chitin synthase III to polarized growth sites in yeast, Mol Biol Cell, 9 (1998) 3383-3397.

[40] E. Nikko, A.M. Marini, B. Andre, Permease recycling and ubiquitination status reveal a particular role for Bro1 in the multivesicular body pathway, J Biol Chem, 278 (2003) 50732-50743.

[41] L. Hicke, B. Zanolari, H. Riezman, Cytoplasmic tail phosphorylation of the alpha-factor receptor is required for its ubiquitination and internalization, J Cell Biol, 141 (1998) 349-358.

[42] K.A. Schandel, D.D. Jenness, Direct evidence for ligand-induced internalization of the yeast alpha-factor pheromone receptor, Mol Cell Biol, 14 (1994) 7245-7255.

[43] L. Hicke, H. Riezman, Ubiquitination of a yeast plasma membrane receptor signals its ligand-stimulated endocytosis, Cell, 84 (1996) 277-287.

[44] M.C. Overton, K.J. Blumer, G-protein-coupled receptors function as oligomers in vivo, Curr Biol, 10 (2000) 341-344.

[45] A. Yesilaltay, D.D. Jenness, Homo-oligomeric complexes of the yeast alpha-factor pheromone receptor are functional units of endocytosis, Mol Biol Cell, 11 (2000) 2873-2884.

[46] M.C. Overton, S.L. Chinault, K.J. Blumer, Oligomerization, biogenesis, and signaling is promoted by a glycophorin A-like dimerization motif in transmembrane domain 1 of a yeast G protein-coupled receptor, J Biol Chem, 278 (2003) 49369-49377.

[47] B. Antonny, I. Huber, S. Paris, M. Chabre, D. Cassel, Activation of ADP-ribosylation factor 1 GTPase-activating protein by phosphatidylcholine-derived

diacylglycerols, J Biol Chem, 272 (1997) 30848-30851.

[48] A. Spang, Y. Shiba, P.A. Randazzo, Arf GAPs: gatekeepers of vesicle generation, FEBS Lett, 584 (2010) 2646-2651.

[49] M.K. Min, M. Jang, M. Lee, J. Lee, K. Song, Y. Lee, K.Y. Choi, D.G. Robinson, I. Hwang, Recruitment of Arf1-GDP to Golgi by Glo3p-type ArfGAPs is crucial for golgi maintenance and plant growth, Plant Physiol, 161 (2013) 676-691.

[50] J. Lachmann, F.A. Barr, C. Ungermann, The Msb3/Gyp3 GAP controls the activity of the Rab GTPases Vps21 and Ypt7 at endosomes and vacuoles, Mol Biol Cell, 23 (2012) 2516-2526.

[51] D.P. Nickerson, M.R. Russell, S.Y. Lo, H.C. Chapin, J.M. Milnes, A.J. Merz, Termination of isoform-selective Vps21/Rab5 signaling at endolysosomal organelles by Msb3/Gyp3, Traffic, 13 (2012) 1411-1428.

[52] S. Springer, A. Spang, R. Schekman, A primer on vesicle budding, Cell, 97 (1999) 145-148.

[53] U. Rein, U. Andag, R. Duden, H.D. Schmitt, A. Spang, ARF-GAP-mediated interaction between the ER-Golgi v-SNAREs and the COPI coat, J Cell Biol, 157 (2002) 395-404.

[54] M. Robinson, P.P. Poon, C. Schindler, L.E. Murray, R. Kama, G. Gabriely, R.A. Singer, A. Spang, G.C. Johnston, J.E. Gerst, The Gcs1 Arf-GAP mediates Snc1,2 v-SNARE retrieval to the Golgi in yeast, Mol Biol Cell, 17 (2006) 1845-1858.

[55] C. Schindler, A. Spang, Interaction of SNAREs with ArfGAPs precedes recruitment of Sec18p/NSF, Mol Biol Cell, 18 (2007) 2852-2863.

[56] E. Harsay, R. Schekman, A subset of yeast vacuolar protein sorting mutants is blocked in one branch of the exocytic pathway, J Cell Biol, 156 (2002) 271-285.

[57] S. Gurunathan, D. David, J.E. Gerst, Dynamin and clathrin are required for the biogenesis of a distinct class of secretory vesicles in yeast, Embo J, 21 (2002) 602-614.

[58] E. Harsay, A. Bretscher, Parallel secretory pathways to the cell surface in yeast, J Cell Biol, 131 (1995) 297-310.

[59] R.M. Barfield, J.C. Fromme, R. Schekman, The exomer coat complex transports Fus1p to the plasma membrane via a novel plasma membrane sorting signal in yeast, Mol Biol Cell, 20 (2009) 4985-4996.

[60] B. Santos, A. Duran, M.H. Valdivieso, CHS5, a gene involved in chitin synthesis

and mating in Saccharomyces cerevisiae, Mol Cell Biol, 17 (1997) 2485-2496.

Supplementary Fig. 1. Verification of the yeast deletion strains. Cells depleted of Arf-GAP, Rab-GAP, or Rho-GAP were purchased from Open Biosystems and strain identities were confirmed by PCR using primers specific to the target gene and the selection marker. Wild-type parental strains were used as negative controls.

Supplementary Fig. 2. Delays of α-factor internalization and transport in *glo3*Δ cells. (**A**) Wild-type or *glo3*Δ cells expressing Pep4-GFP were treated with A594-α-factor, and images were acquired 15 min after washing out unbound A594-α-factor and warming the cell to 25°C. Each panel shows a representative image of A594-α-factor localization in wild-type and *glo3*Δ cells which was categorized as plasma membrane (PM), endosome and vacuole (endosome + vacuole), or vacuole only (vacuole). Arrowheads indicate examples of A594-α-factor being localized at endosomes. Scale bars, 2.5 μm. (**B**) Each curve represents the amount (cpm) of ^{35}S-labeled α-factor internalized into the indicated strains at each time point. The amount of internalized α-factor indicates the radioactive ^{35}S signal of cells that were washed with a pH 1.1 buffer to remove surface-bound ^{35}S-α-factor. Each experiment was performed at least three times.

Figure 1

Click here to download high resolution image

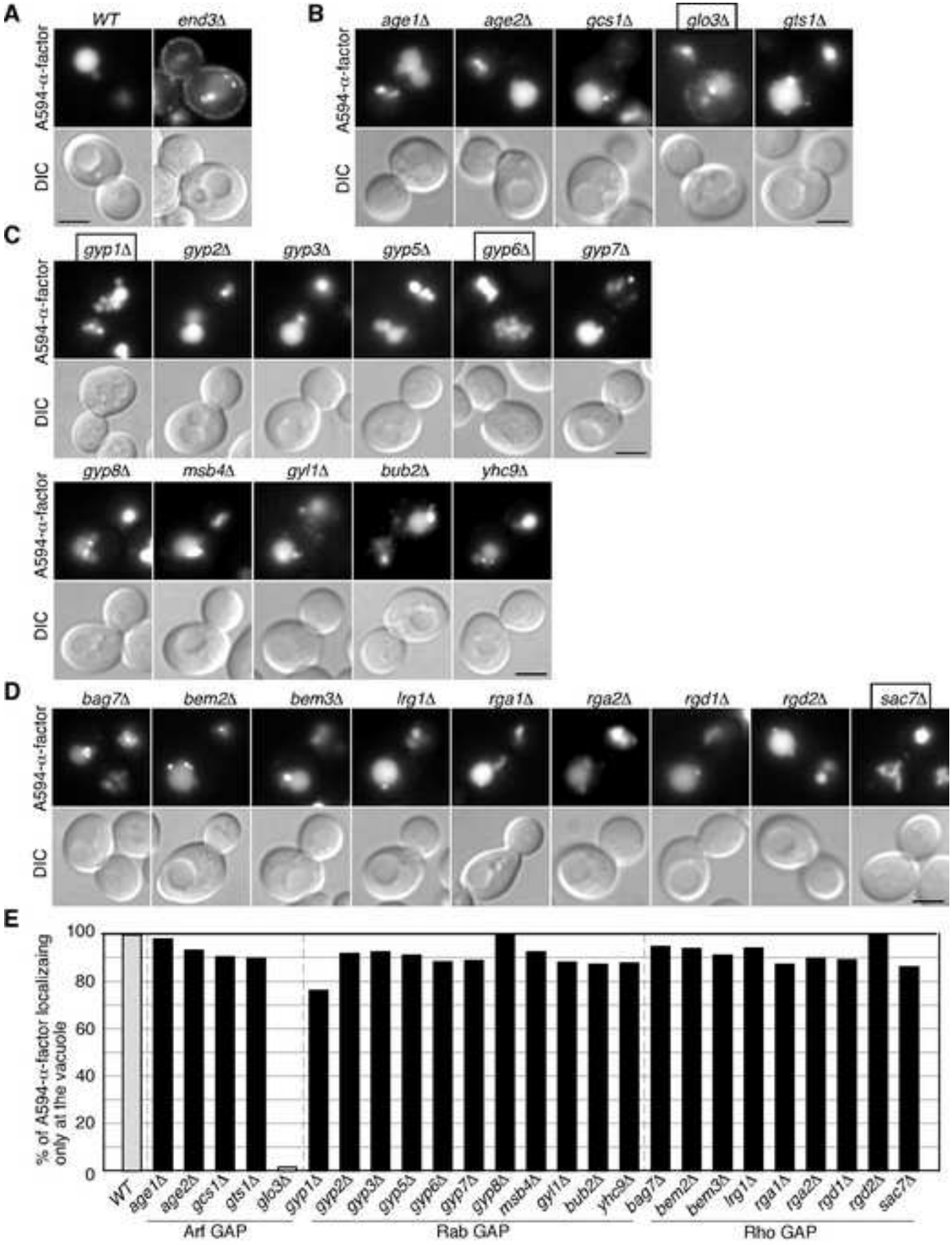

Figure 1. Kawada et al.

Figure 2

Click here to download high resolution image

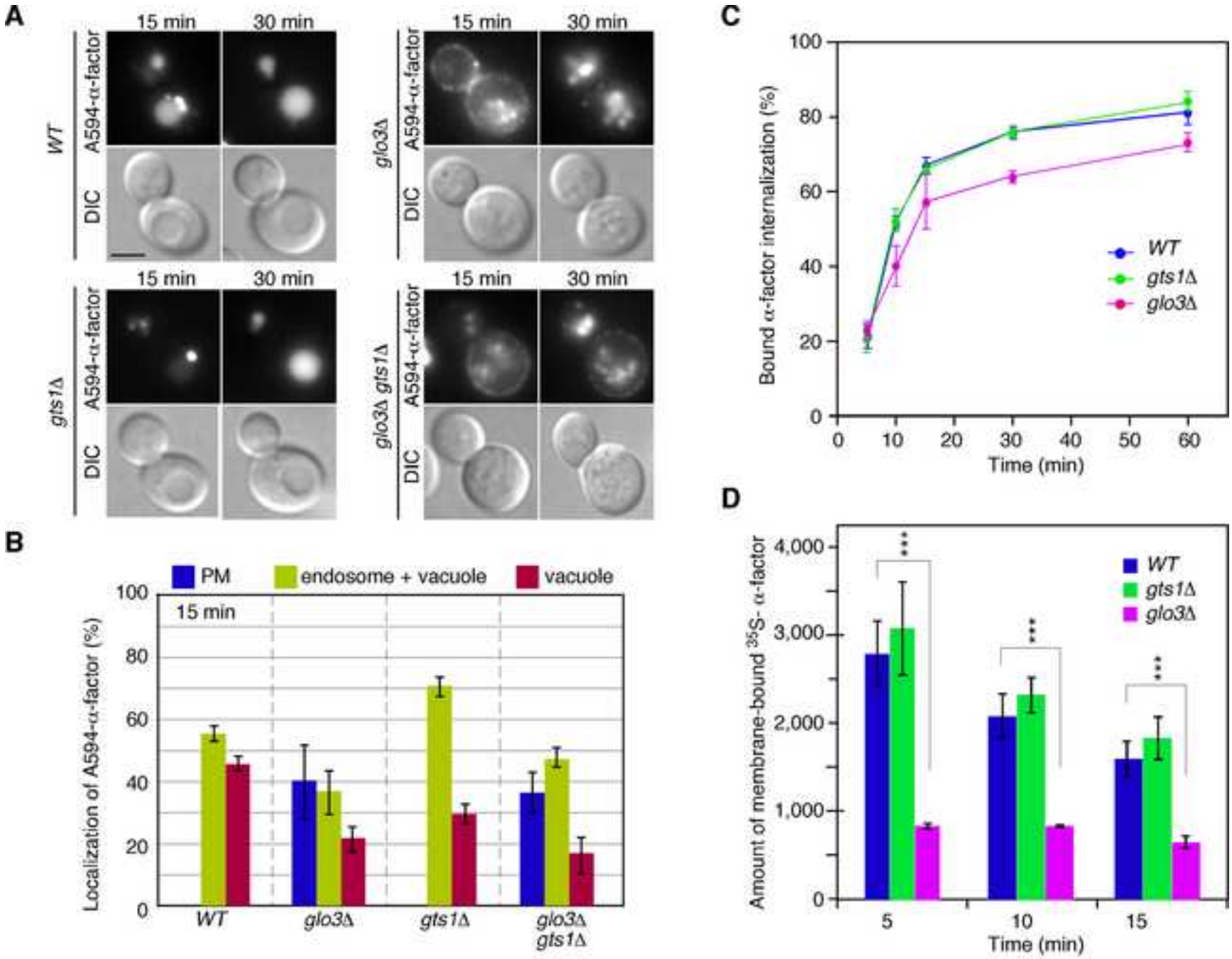

Figure 2. Kawada et al.

Figure 3
Click here to download high resolution image

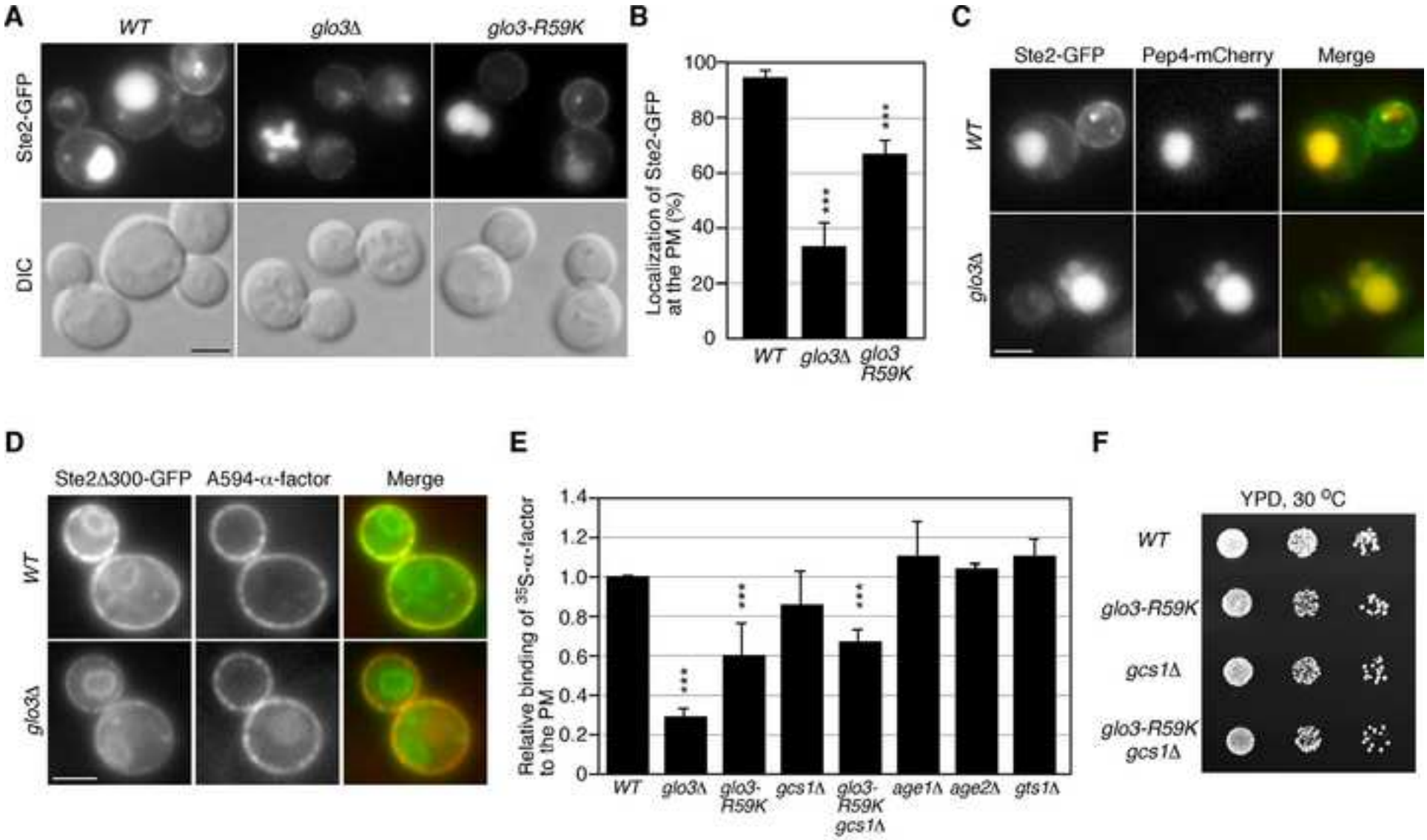

Figure 3. Kawada et al.

Figure 4

Click here to download high resolution image

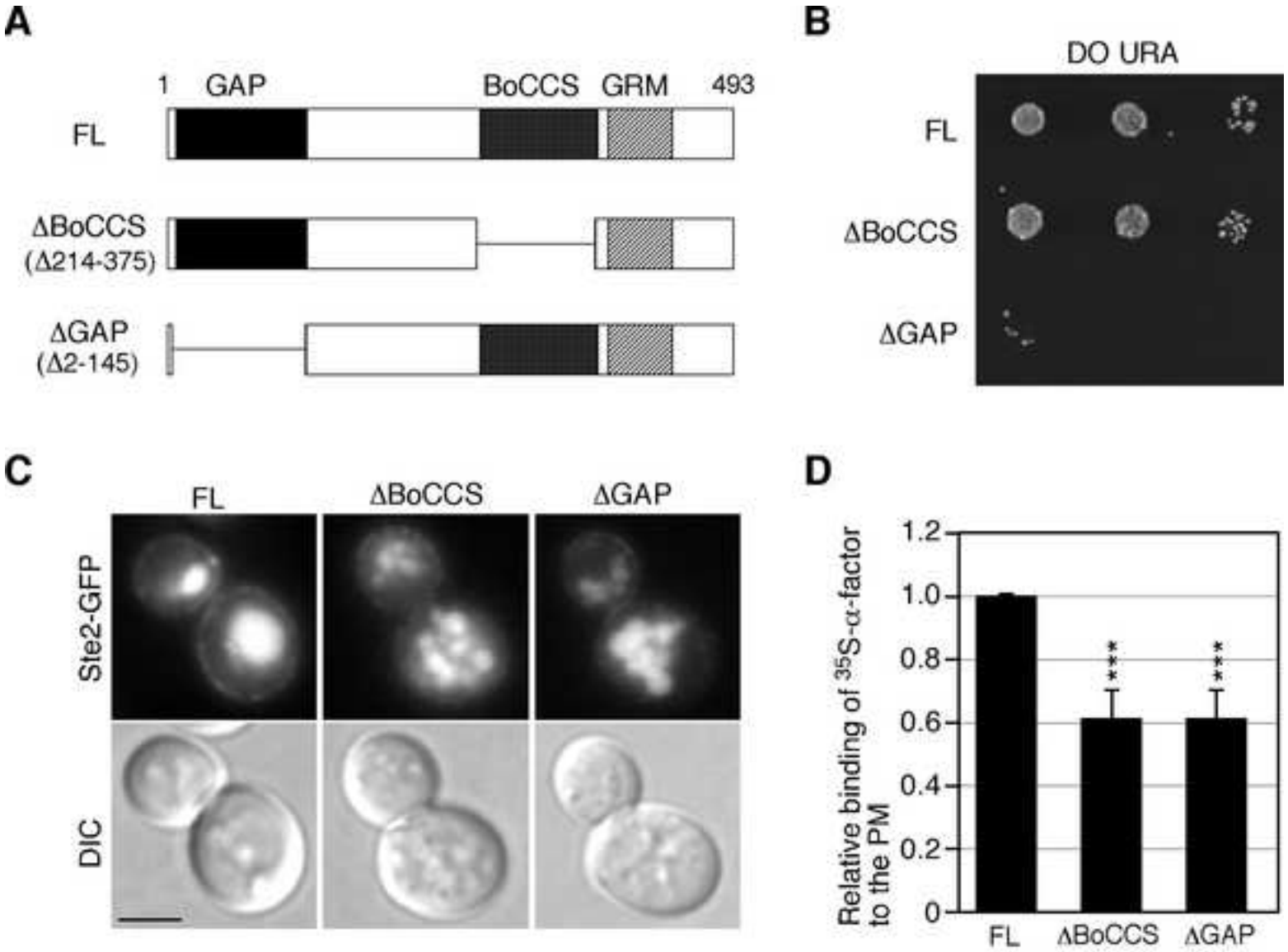

Figure 4. Kawada et al.

Figure 5

Click here to download high resolution image

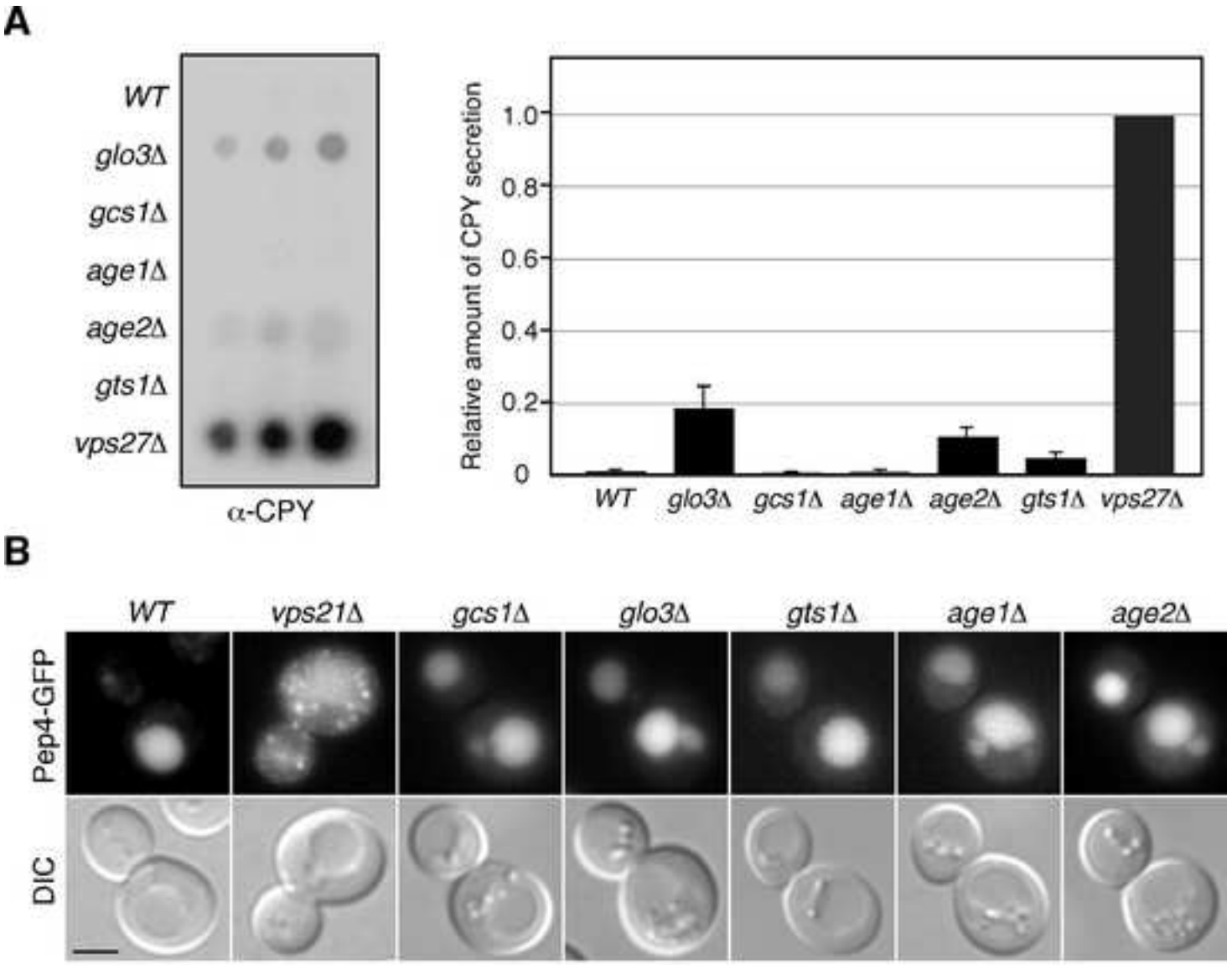

Figure 5. Kawada et al.

Figure 6

Click here to download high resolution image

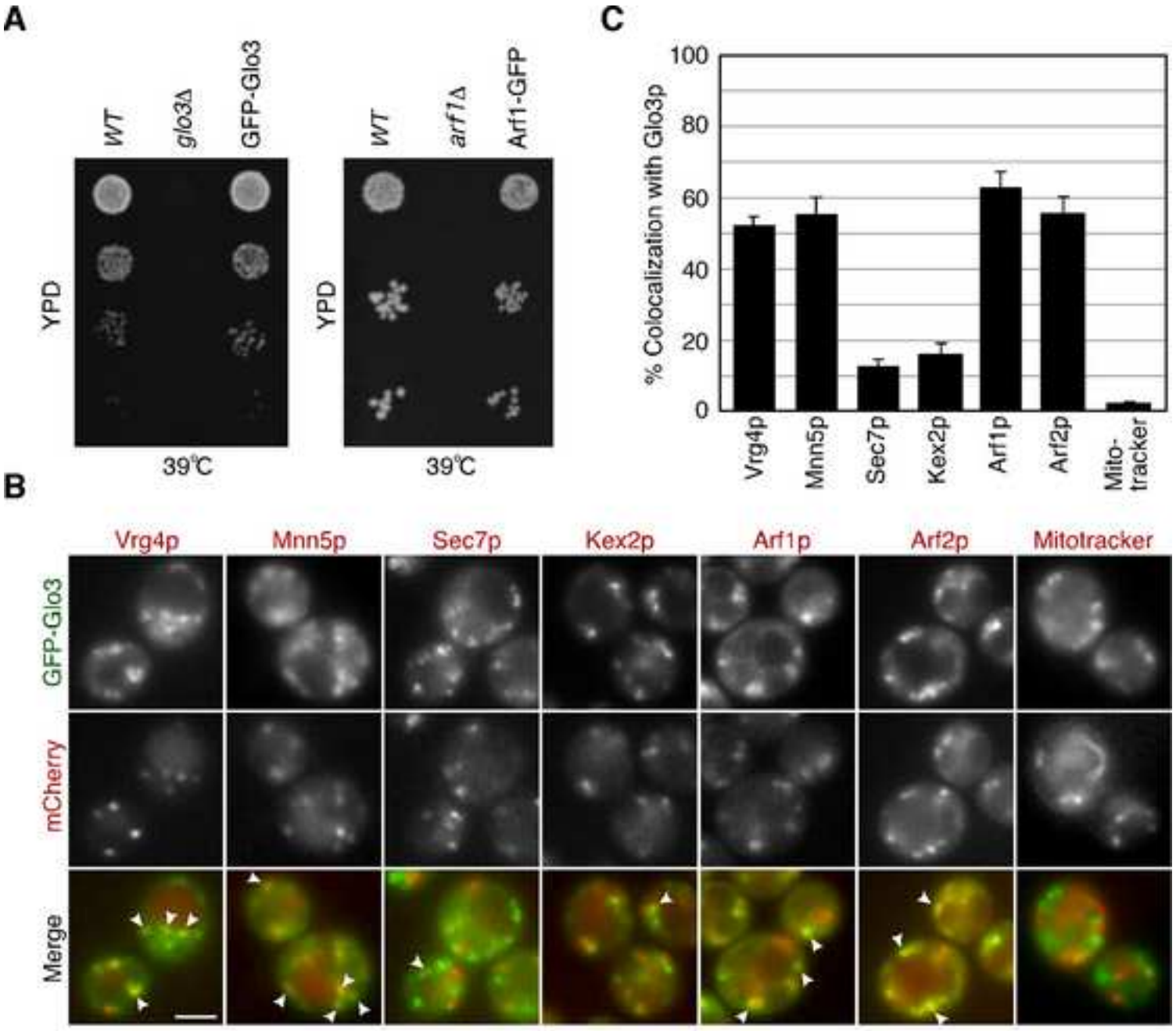

Figure 6. Kawada et al.

Figure 7

Click here to download high resolution image

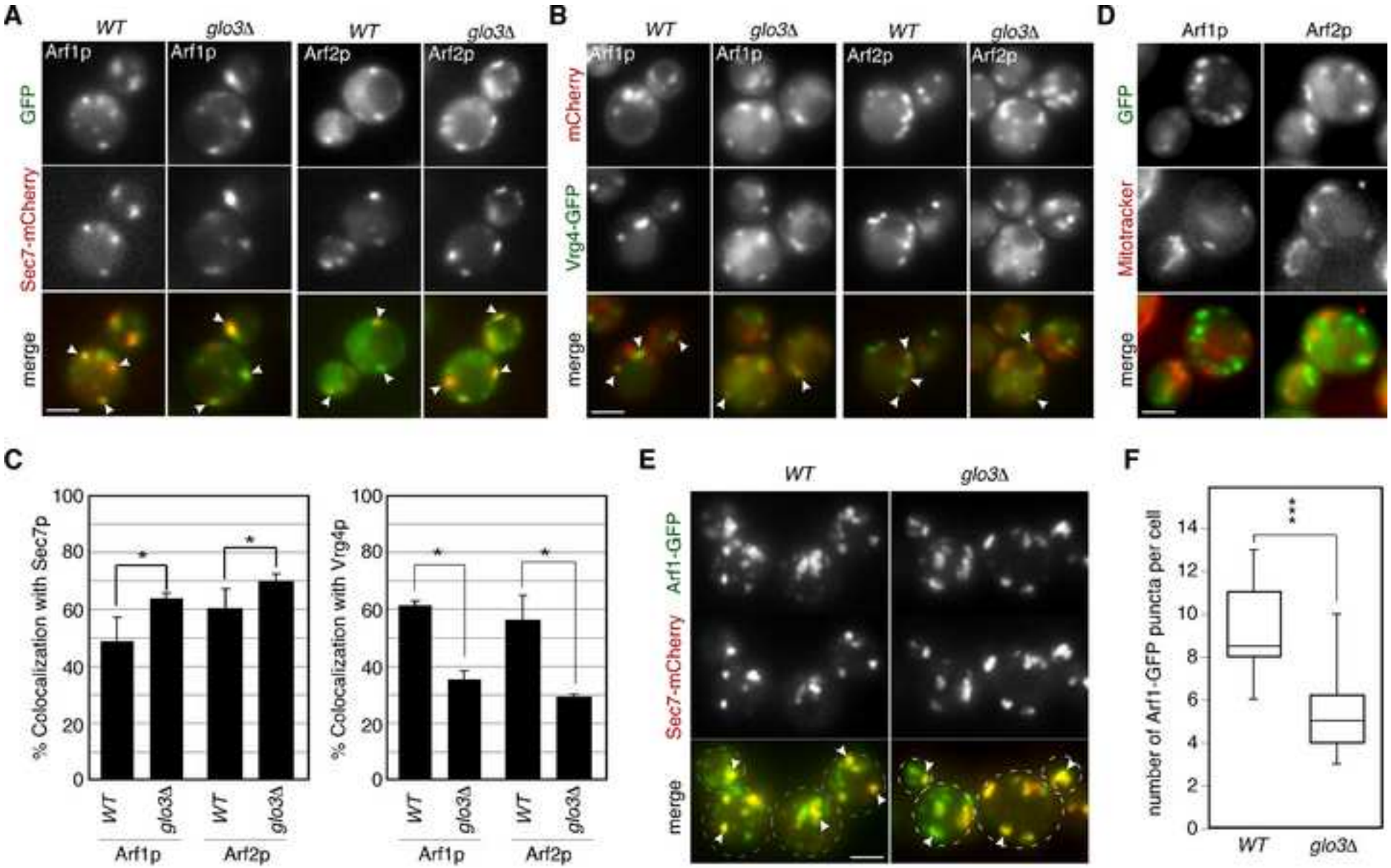

Figure 7. Kawada et al.

Figure 8

Click here to download high resolution image

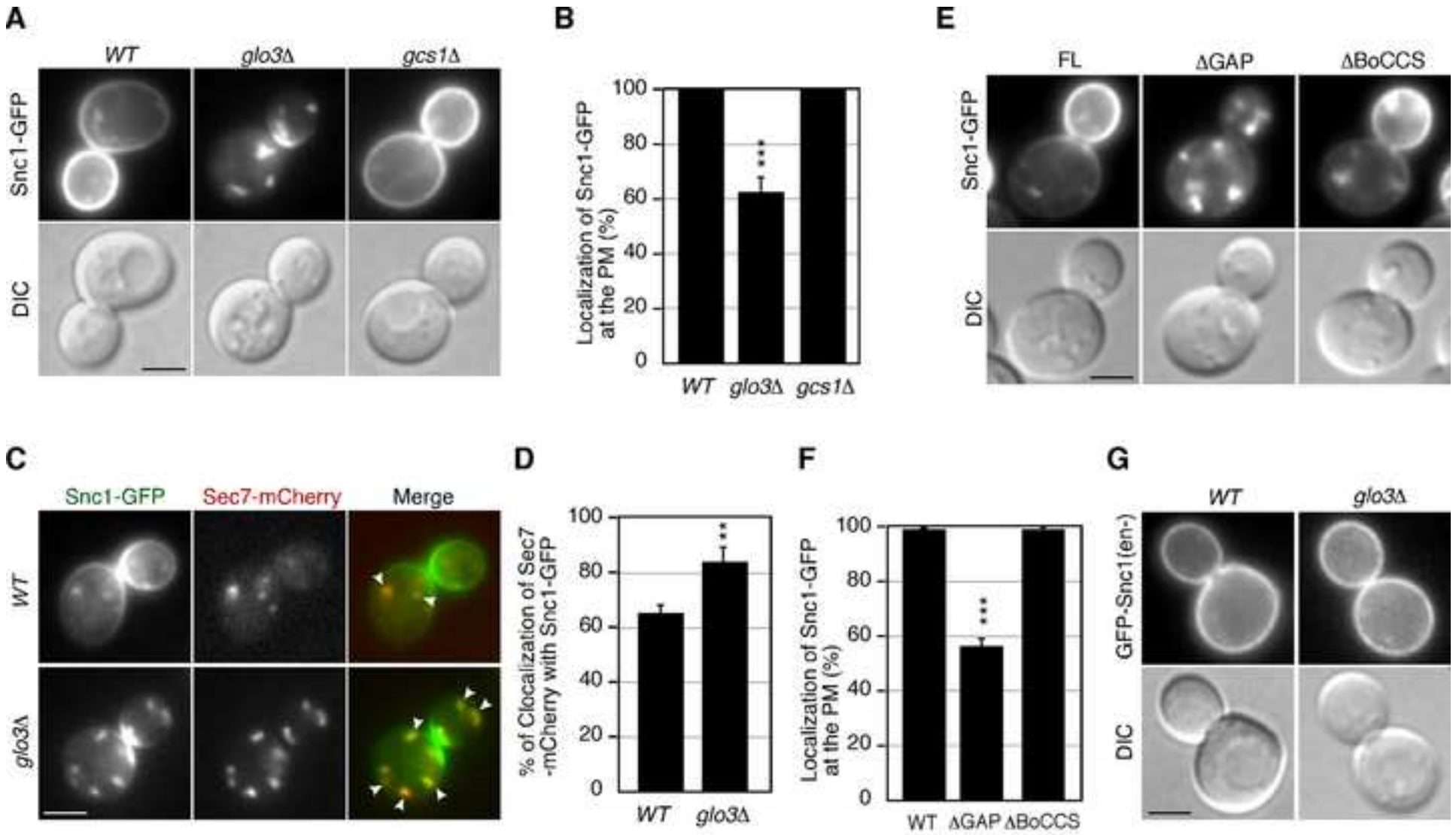

Figure 8. Kawada et al.

Figure 9

Click here to download high resolution image

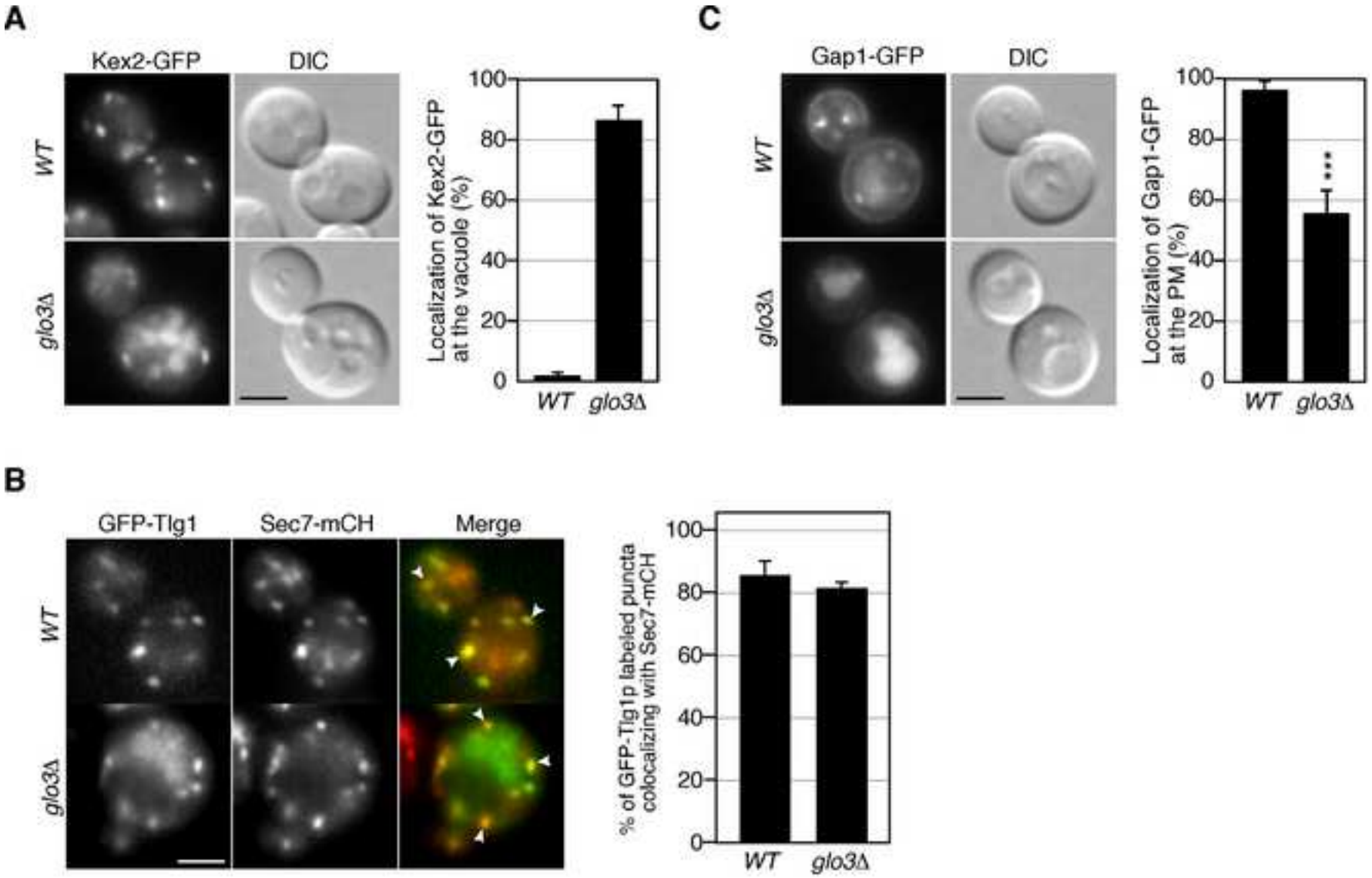

Figure 9. Kawada et al.

Figure 10
Click here to download high resolution image

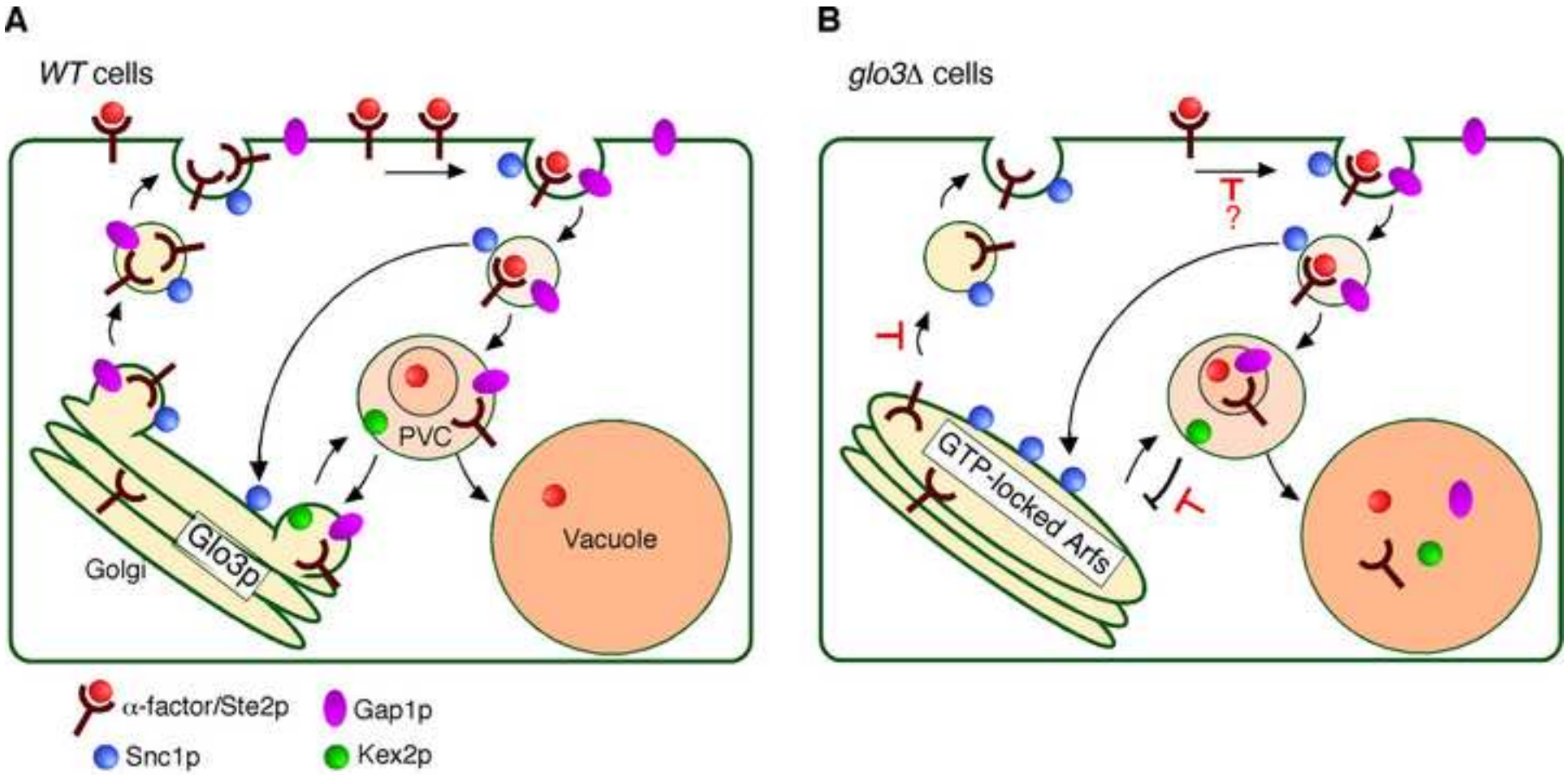

Figure 10. Kawada et al.

Table 1. Yeast Strains

Strain	Genotype	Source
JJTY0059[a]	*Mat***a** *his3-Δ200 leu2-3, 112 ura3-52 bar1Δ::LEU2*	Toshima lab
JJTY1210[a]	*Matα his3-Δ200 leu2-3, 112 ura3-52 lys2-801 PEP4-3GFP::HIS3*	Toshima lab
JJTY1641[a]	*Matα his3-Δ200 leu2-3, 112 ura3-52 lys2-801 SNC1-GFP::HIS3*	Toshima lab
JJTY1681[b]	*Mat***a** *his3Δ1 leu2Δ0 met15Δ0 ura3Δ0 age1Δ::KanMX PEP4-GFP::HIS3*	This study
JJTY1682[b]	*Mat***a** *his3Δ1 leu2Δ0 met15Δ0 ura3Δ0 age2Δ::KanMX PEP4-GFP::HIS3*	This study
JJTY1687[b]	*Mat***a** *his3Δ1 leu2Δ0 met15Δ0 ura3Δ0 gcs1Δ::KanMX PEP4-GFP::HIS3*	This study
JJTY1688[b]	*Mat***a** *his3Δ1 leu2Δ0 met15Δ0 ura3Δ0 glo3Δ::KanMX PEP4-GFP::HIS3*	This study
JJTY1689[b]	*Mat***a** *his3Δ1 leu2Δ0 met15Δ0 ura3Δ0 gts1Δ::KanMX PEP4-GFP::HIS3*	This study
JJTY2272[b]	*Mat***a** *his3Δ1 leu2Δ0 met15Δ0 ura3Δ0 gcs1Δ::KanMX SNC1-GFP::HIS3*	This study
JJTY2273[b]	*Mat***a** *his3Δ1 leu2Δ0 met15Δ0 ura3Δ0 glo3Δ::KanMX SNC1-GFP::HIS3*	This study
JJTY3247[b]	*Mat***a** *his3Δ1 leu2Δ0 ura3Δ0 me15Δ0 bar1Δ::LEU2 glo3Δ::KanMX6*	This study
JJTY3378[b]	*Mat***a** *his3Δ1 leu2Δ0 ura3Δ0 met15Δ0 age1Δ::KanMX bar1Δ::LEU2*	This study
JJTY3379[b]	*Mat***a** *his3Δ1 leu2Δ0 ura3Δ0 met15Δ0 age2Δ::KanMX bar1Δ::LEU2*	This study
JJTY3380[b]	*Mat***a** *his3Δ1 leu2Δ0 ura3Δ0 met15Δ0 gcs1Δ::KanMX bar1Δ::LEU2*	This study
JJTY3381[b]	*Mat***a** *his3Δ1 leu2Δ0 ura3Δ0 met15Δ0 gts1Δ::KanMX bar1Δ::LEU2*	This study
JJTY3382[b]	*Mat***a** *his3Δ1 leu2Δ0 ura3Δ0 met15Δ0 glo3Δ::KanMX gts1Δ::KanMX bar1Δ::LEU2*	This study
JJTY3392[b]	*Mat***a** *his3Δ1 leu2Δ0 ura3Δ0 met15Δ0 ARF1-GFP::HIS3 SEC7-mCherry::URA3*	This study
JJTY3393[b]	*Mat***a** *his3Δ1 leu2Δ0 ura3Δ0 met15Δ0 ARF2-GFP::HIS3 SEC7-mCherry::URA3*	This study
JJTY3394[b]	*Mat***a** *his3Δ1 leu2Δ0 ura3Δ0 met15Δ0 glo3Δ::KanMX ARF1-GFP::HIS3 SEC7-mCherry::URA3*	This study
JJTY3395[b]	*Mat***a** *his3Δ1 leu2Δ0 ura3Δ0 met15Δ0 glo3Δ::KanMX ARF2-GFP::HIS3 SEC7-mCherry::URA3*	This study
JJTY3396[b]	*Mat***a** *his3Δ1 leu2Δ0 ura3Δ0 met15Δ0 STE2-GFP::HIS3*	This study
JJTY3397[b]	*Mat***a** *his3Δ1 leu2Δ0 ura3Δ0 met15Δ0 glo3Δ::KanMX STE2-GFP::HIS3*	This study

JJTY3398[b]	*Mat***a** *his3Δ1 leu2Δ0 ura3Δ0 met15Δ0 STE2-GFP*::*HIS3 PEP4-mCherry*::*URA3*	This study
JJTY3399[b]	*Mat***a** *his3Δ1 leu2Δ0 ura3Δ0 met15Δ0 glo3Δ*::*KanMX STE2-GFP*::*HIS3 PEP4-mCherry*::*URA3*	This study
JJTY3402[b]	*Mat***a** *his3Δ1 leu2Δ0 ura3Δ0 met15Δ0 SNC1-GFP*::*HIS3 SEC7-mCherry*::*URA3*	This study
JJTY3403[b]	*Mat***a** *his3Δ1 leu2Δ0 ura3Δ0 met15Δ0 glo3Δ*::*KanMX SNC1-GFP*::*HIS3 SEC7-mCherry*::*URA3*	This study
JJTY3404[b]	*Mat***a** *his3Δ1 leu2Δ0 ura3Δ0 met15Δ0 end3Δ*::*LEU2 STE2-GFP*::*HIS3*	This study
JJTY3405[b]	*Mat***a** *his3Δ1 leu2Δ0 ura3Δ0 met15Δ0 glo3Δ*::*KanMX end3Δ*::*LEU2 STE2-GFP*::*HIS3*	This study
JJTY3413[b]	*Mat***a** *his3Δ1 leu2Δ0 ura3Δ0 met15Δ0 HA-glo3R59K*::*HIS3 STE2-GFP*::*HIS3*	This study
JJTY3414[b]	*Mat***a** *his3Δ1 leu2Δ0 ura3Δ0 met15Δ0 HA-glo3R59K*::*HIS3 bar1Δ*::*LEU2*	This study
JJTY3415[b]	*Mat***a** *his3Δ1 leu2Δ0 ura3Δ0 met15Δ0 GFP-GLO3*::*HIS3*	This study
JJTY3416[b]	*Mat***a** *his3Δ1 leu2Δ0 ura3Δ0 met15Δ0 GFP-GLO3*::*HIS3 SEC7-mCherry*::*URA3*	This study
JJTY3572[b]	*Mat***a** *his3Δ1 leu2Δ0 ura3Δ0 met15Δ0 GFP-GLO3*::*HIS3 VRG4-mCherry*::*URA3*	This study
JJTY3573[b]	*Mat***a** *his3Δ1 leu2Δ0 ura3Δ0 met15Δ0 GFP-GLO3*::*HIS3 MNN5-mCherry*::*URA3*	This study
JJTY3574[b]	*Mat***a** *his3Δ1 leu2Δ0 ura3Δ0 met15Δ0 GFP-GLO3*::*HIS3 KEX2-mCherry*::*URA3*	This study
JJTY3575[b]	*Mat***a** *his3Δ1 leu2Δ0 ura3Δ0 met15Δ0 GFP-GLO3*::*HIS3 ARF1-mCherry*::*URA3*	This study
JJTY3576[b]	*Mat***a** *his3Δ1 leu2Δ0 ura3Δ0 met15Δ0 GFP-GLO3*::*HIS3 ARF2-mCherry*::*URA3*	This study
JJTY3392[b]	*Mat***a** *his3Δ1 leu2Δ0 ura3Δ0 met15Δ0 ARF1-GFP*::*HIS3 SEC7-mCherry*::*URA3*	This study
JJTY3393[b]	*Mat***a** *his3Δ1 leu2Δ0 ura3Δ0 met15Δ 0 ARF2-GFP*::*HIS3 SEC7-mCherry*::*URA3*	This study
JJTY3394[b]	*Mat***a** *his3Δ1 leu2Δ0 ura3Δ0 met15Δ0 glo3Δ*::*KanMX ARF1-GFP*::*HIS3 SEC7-mCherry*:*URA3*	This study
JJTY3970[b]	*Mat***a** *his3Δ1 leu2Δ0 ura3Δ0 met15Δ0 ARF1-mCherry*::*URA3 VRG4-GFP*:*HIS3*	This study
JJTY3971[b]	*Mat***a** *his3Δ1 leu2Δ0 ura3Δ0 met15Δ 0 ARF2-mCherry*::*URA3 VRG4-GFP*:*HIS3*	This study
JJTY3972[b]	*Mat***a** *his3Δ1 leu2Δ0 ura3Δ0 met15Δ0 glo3Δ*::*KanMX ARF1-mCherry*::*URA3 VRG4-GFP*:*HIS3*	This study
JJTY4781[b]	*Mat***a** *his3Δ1 leu2Δ0 ura3Δ0 met15Δ0 bar1Δ*::*LEU2 glo3Δ* ::*KanMX6 KEX2-GFP*::*HIS3*	This study
JJTY4782[b]	*Mat***a** *his3Δ1 leu2Δ0 ura3Δ0 met15Δ0 bar1Δ*::*LEU2 glo3Δ* ::*KanMX6 GAP1-GFP*::*HIS3*	This study

JJTY4783[b]	*Mat***a** *his3Δ1 leu2Δ0 ura3Δ0 met15Δ0 bar1Δ*::*LEU2 glo3Δ* ::*KanMX6 SEC7-mCherry*::*URA* [pRS313-*GFP-TLG1*]	This study
JJTY4785[b]	*Mat***a** *his3Δ1 leu2Δ0 ura3Δ0 met15Δ0 bar1Δ*::*LEU2 glo3Δ* ::*KanMX6 STE2Δ300-GFP*::*HIS3*	This study
JJTY4786[b]	*Mat***a** *his3Δ1 leu2Δ0 ura3Δ0 met15Δ0 KEX2-GFP*::*HIS3*	This study
JJTY4787[b]	*Mat***a** *his3Δ1 leu2Δ0 ura3Δ0 met15Δ0 GAP1-GFP*::*HIS3*	This study
JJTY4790[b]	*Mat***a** *his3Δ1 leu2Δ0 ura3Δ0 met15Δ0 bar1Δ*::*LEU2 STE2Δ300-GFP*::*HIS3*	This study
JJTY4791[b]	*Mat***a** *his3Δ1 leu2Δ0 ura3Δ0 met15Δ0 bar1Δ*::*LEU2 gcs1Δ* ::*KanMX6 HA-glo3R59K*::*HIS3*	This study
JJTY4784[b]	*Mat***a** *his3Δ1 leu2Δ0 ura3Δ0 met15Δ0 bar1Δ*::*LEU2 glo3Δ* ::*KanMX6* [pRS426-*Snc1en-GFP*]	This study
JJTY4788[b]	*Mat***a** *his3Δ1 leu2Δ0 ura3Δ0 met15Δ0 SEC7-mCherry*::*URA3* [pRS313-*GFP-TLG1*]	This study
JJTY4789[b]	*Mat***a** *his3Δ1 leu2Δ0 ura3Δ0 met15Δ0* [pRS426-*Snc1en-GFP*]	This study
JJTY5143[b]	*Mat***a** *his3Δ1 leu2Δ0 ura3Δ0 me15Δ0 bar1Δ*::*LEU2 glo3Δ*::*KanMX6* [pRS316-*GLO3*]	This study
JJTY5144[b]	*Mat***a** *his3Δ1 leu2Δ0 ura3Δ0 me15Δ0 bar1Δ*::*LEU2 glo3Δ*::*KanMX6* [pRS316-*GLO3ΔGAP*]	This study
JJTY5145[b]	*Mat***a** *his3Δ1 leu2Δ0 ura3Δ0 me15Δ0 bar1Δ*::*LEU2 glo3Δ*::*KanMX6* [pRS316-*GLO3ΔBoCCS*]	This study
JJTY5146[b]	*Mat***a** *his3Δ1 leu2Δ0 ura3Δ0 met15Δ0 glo3Δ*::*KanMX STE2-GFP*::*HIS3* [pRS316-*GLO3*]	This study
JJTY5147[b]	*Mat***a** *his3Δ1 leu2Δ0 ura3Δ0 met15Δ0 glo3Δ*::*KanMX STE2-GFP*::*HIS3* [pRS316-*GLO3ΔGAP*]	This study
JJTY5148[b]	*Mat***a** *his3Δ1 leu2Δ0 ura3Δ0 met15Δ0 glo3Δ*::*KanMX STE2-GFP*::*HIS3* [pRS316-*GLO3ΔBoCCS*]	This study
JJTY5149[b]	*Mat***a** *his3Δ1 leu2Δ0 met15Δ0 ura3Δ0 glo3Δ::KanMX SNC1-GFP*::*HIS3* [pRS316-*GLO3*]	This study
JJTY5150[b]	*Mat***a** *his3Δ1 leu2Δ0 met15Δ0 ura3Δ0 glo3Δ::KanMX SNC1-GFP*::*HIS3* [pRS316-*GLO3ΔGAP*]	This study
JJTY5151[b]	*Mat***a** *his3Δ1 leu2Δ0 met15Δ0 ura3Δ0 glo3Δ::KanMX SNC1-GFP*::*HIS3* [pRS316-*GLO3ΔBoCCS*]	This study

[a]Derived from strain S288C. [b]Derived from strain BY4741.

Supplementary Figure 1
Click here to download high resolution image

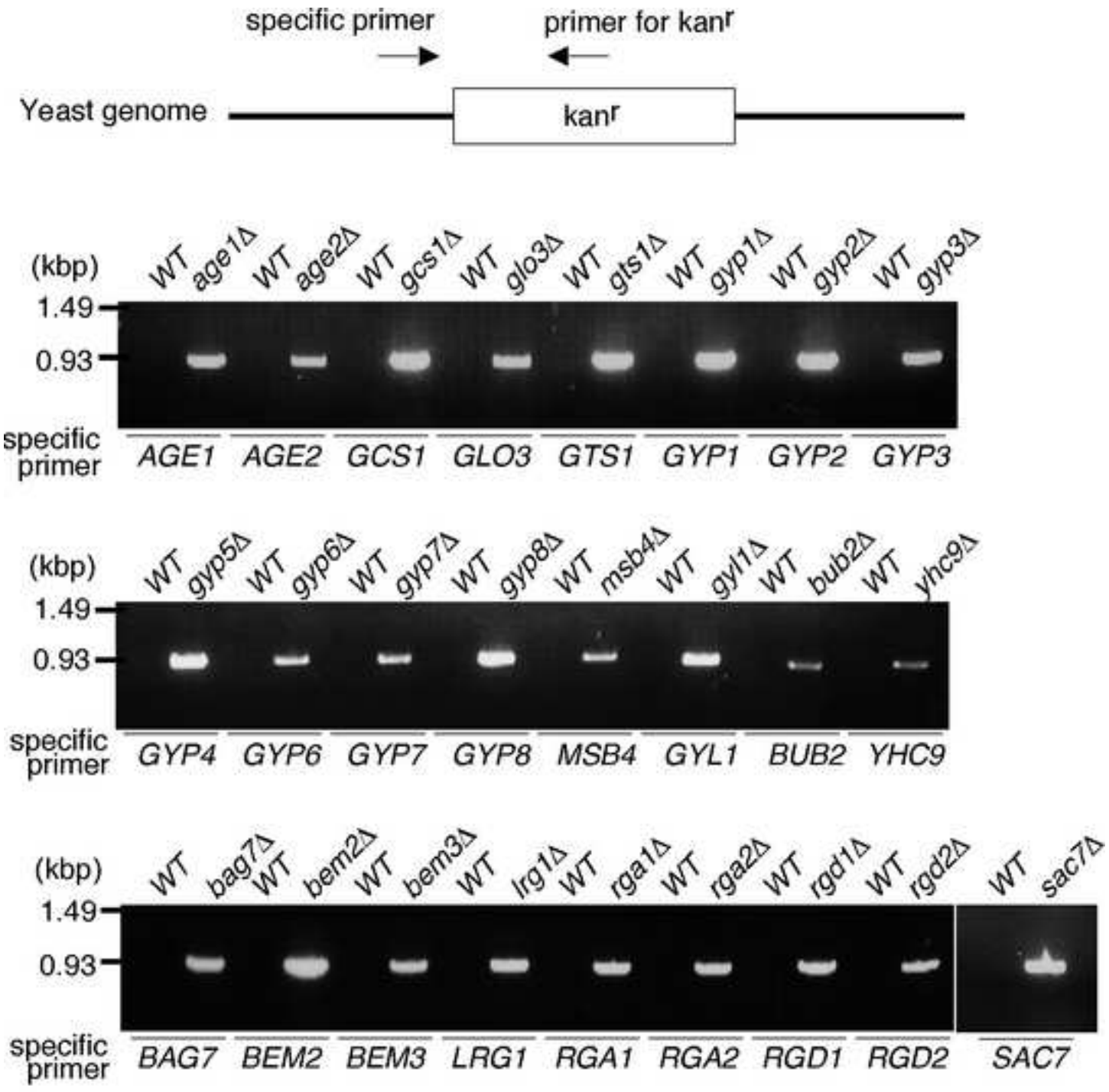

Supplementary Figure 1. Kawada et al.

Supplementary Figure 2

Click here to download high resolution image

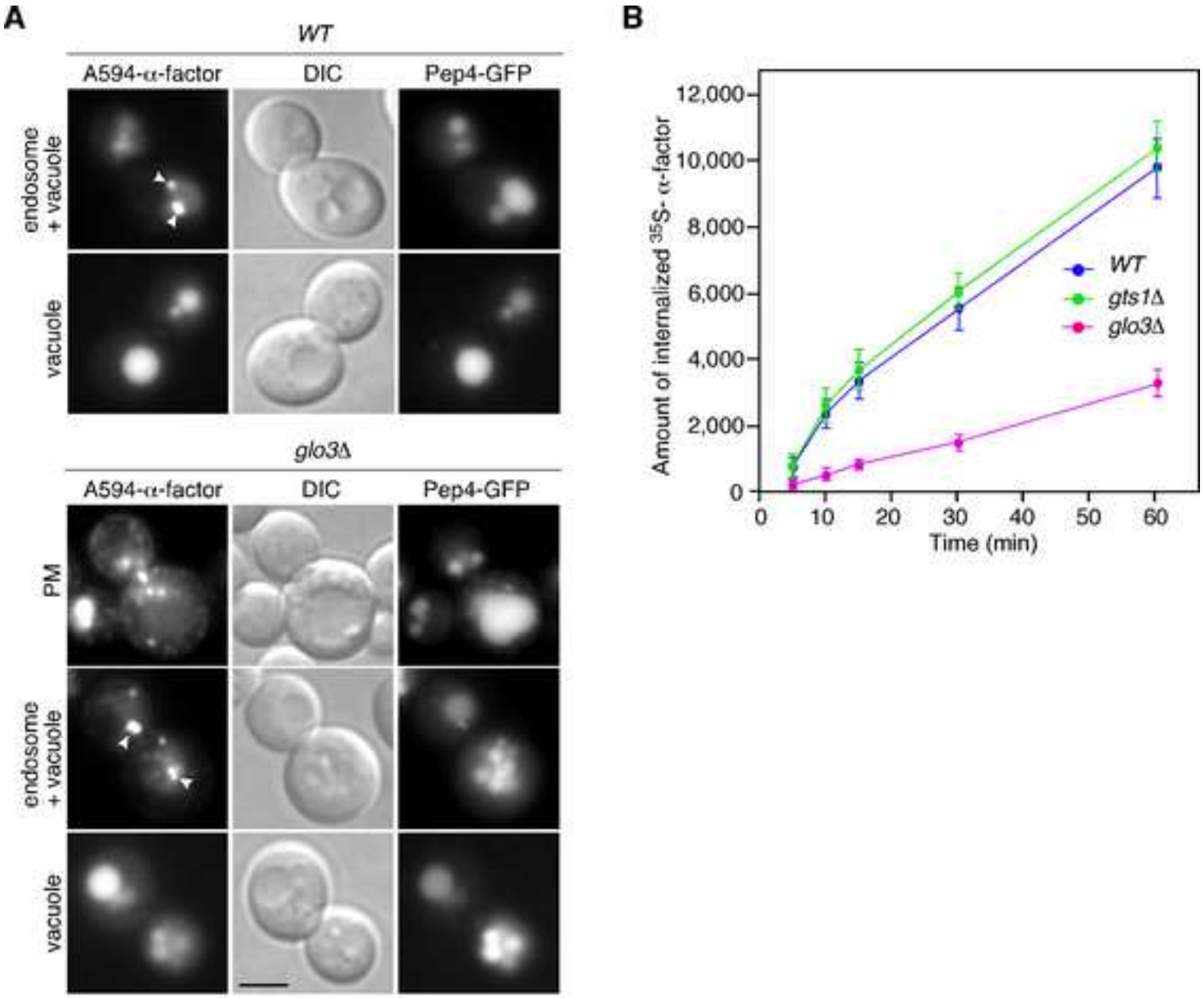

Supplementary Figure 2. Kawada et al.